Universidad Nacional de Mar del Plata- Facultad de Ingeniería

Friedrich-Alexander Universität Erlangen-Nürnberg

"FABRICATION AND CHARACTERIZATION OF ELECTROSPUN ZEIN-BASED SCAFFOLDS FOR SOFT TISSUE ENGINEERING"

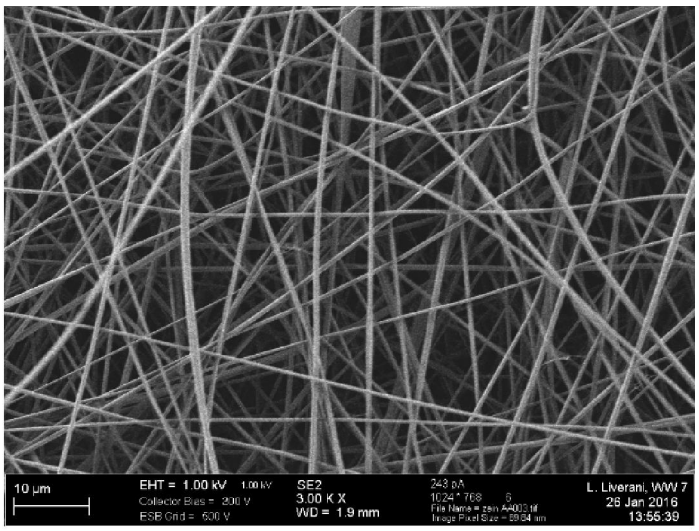

B

AGUSTINA MASSONE

DIRECTORS: DRA. LILIANA LIVERANI

DR. GUSTAVO ABRAHAM

Index

List of Figures

List of Tables

1. Summary

Nanofibers and nanomaterials are potentially recent additions to materials in relation to tissue engineering (TE). TE involves the regeneration of biological tissues, which are damaged, using cells with the aid of supporting structures and biomolecules. Mimicking the architecture and functions of extracellular matrix is one of the challenges for TE. Conventional treatments, such as transplantations and the use of mechanical assist devices, could be replaced with this approach. Electrospinning is a versatile and simple technique to produce polymer fibers with diameters varying from 5 nm to 5 μm, which can mimic the extracellular matrix. This characteristic stimulates the expression of specific signals and, in combination with growth factors and proteins, has an important influence in cellular activity. Blending synthetic with natural polymers, combine the advantages of both leading to good biodegradation and mechanical properties, and excellent cell adhesion and growth.

In this work, it is presented the preparation and characterization of natural polymer (zein)-based nanofibrous scaffolds obtained through electrospinning technique. The processing parameters were adjusted to obtain randomly-oriented nanofibrous mats. Although the basic principles of the technique are simple, the many factors and parameters involved in it make the process complex. Through the analysis of testing results, it was found that the blend of zein with synthetic polymers improve in many folds its properties. The nanofibrous mats are of great interest for its applications in tissue engineering.

2. Introduction

2.1 Tissue engineering

Tissue damage or loss due to congenital diseases, trauma, or accidents and end-stage organ failures are the two major causes of illness and death world-wide. Nowadays, approximately a quarter of patients in need of organ transplant die while waiting for a suitable donor. The current demand for transplant organs and tissues is far outpacing the supply, and all projections indicate that this gap will continue to widen. The treatment modalities conventionally employed for these are the transplantation of tissues and organs (autograft, allograft/xenograft) or the use of mechanical assist devices.

Although these approaches significantly improve patient survival, they suffer from serious limitations. Autografts (tissue isolated from the same patient) possess limitations such as donor-site morbidity due to infections and hematomas, as well as the associated risk of infection and limited availability. Allografts (tissue or organ isolated from another individual of the same specie) and xenograft (tissue or organ isolated from another species) possess serious constraints due to immunological incompatibility and the consequent risk of rejection by the body, which necessitates the patients undergoing lifelong immunosuppression treatment. Further they have increased risk of infection, viral disease transmission, tumor development, and many associated side effects. Moreover, tissue or organ transplantation is highly expensive and a complex surgery. On the other hand, the success of mechanical replacement devices or total artificial organs is seriously limited by thromboembolism (formation in a blood vessel of a thrombus that breaks loose and is carried by the blood stream to plug another vessel) associated with infections and durability [(1)].

Tissue engineering (TE), is an important emerging topic in biomedical engineering which has shown a tremendous promise in creating biological alternatives for harvested tissues, implants and prostheses. While tissue engineering focuses on the ability to repair a specific tissue, regenerative engineering aims to regenerate or reconstruct complex tissues and biological systems, such as the whole human limb. Thereby, TE aims to regenerate damaged tissues, instead of replacing them, by developing biological substitutes that restore, maintain or improve tissues function. TE is the application of knowledge and expertise from a multidisciplinary field (medicine, biology, engineering and material science) to develop and manufacture products that utilize the combination of matrix scaffolds with viable human cell systems or cell responsive biomolecules derived from such cells; for the repair, restoration or regeneration of cells or tissues damaged by injury, disease, or congenital defects without simulating any immune response [(2)]. The underlying concept of tissue engineering is the belief that cells can be isolated from a patient, and its population then expanded in a cell culture and seeded onto a carrier. The

resulting tissue engineering construct is then grafted back into the same patient to function as the introduced replacement tissue. In this approach, a highly porous artificial extracellular matrix (ECM) or scaffold, is thought to accommodate cells and guide their growth and tissues regeneration in three dimensions [3]. These basic principles of tissue engineering are schematized in Figure 1.

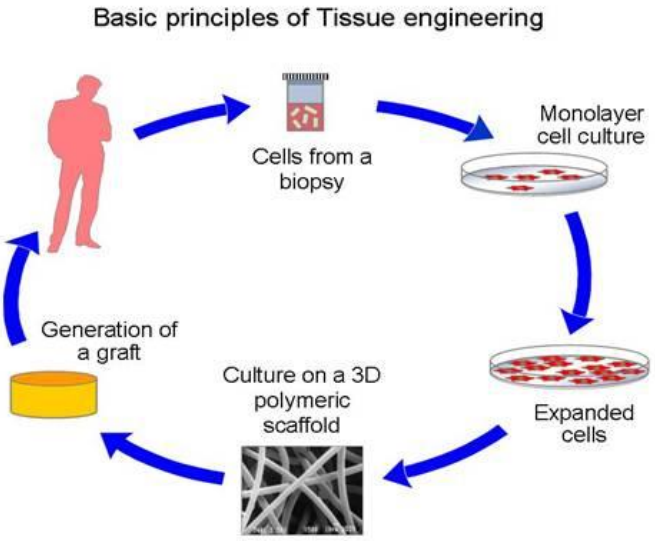

Figure 1. *Basic principles of tissue engineering*

The scaffold structure needs interconnecting pores to allow the 3D flow of culture medium or blood to ensure continuous supply of nutrients and metabolites, which is of great importance for the survival of the cells cultured on the scaffold. The pores should have sizes in the range of 5–10 times of the cell diameter, typically between 100 and 300 µm. Porous scaffolds facilitate tissue formation and provide an adequate mechanical strength required in future during transplantation and implantation in the human body.

TE involves the use of scaffolds or matrices to provide support for cells to express new extracellular matrix. The ECM is the non-cellular component present within all tissues and organs and provides, not only essential physical scaffolding for the cellular constituents, but also initiates crucial biochemical and biomechanical cues that are required for:

- Tissue morphogenesis: Processes by which a tissue takes shape. Such processes involve typically changes in cell number, size, shape and position [4].

- Tissue differentiation: When cells change from one cell type to another.

- Tissue homeostasis: Maintenance of an internal steady state within a defined tissue of an organism, including control of cellular proliferation and death, and control of metabolic function.

The ECM is composed of water, proteins and glycosaminoglycans (GAGs), which are carbohydrate polymers. Each tissue has an ECM with a unique composition and topology. Through its physical and biochemical characteristics, the ECM generates the biochemical and mechanical properties of each organ, such as its tensile and compressive strength and elasticity [5].

2.2 Scaffolds for tissue engineering

Biomaterials play a critical role in tissue engineering by acting as scaffolds. The state of art of biomaterials design has continuously evolved over the past few decades. Biomaterials intended for biomedical applications have the objective of developing artificial materials that can be used to renovate or restore functions of diseased or traumatized tissues in the human body and thus improving the quality of life.

Regardless of the tissue type, several key considerations are important when designing or determining the suitability of a scaffold for use in tissue engineering [1]:

- Biocompatibility: This is the ability of a material to perform with an appropriate host response in a specific application [6]. Cells must adhere, function normally, migrate onto the surface and eventually through the scaffold and begin to proliferate before laying down new matrix. After implantation, the scaffold or tissue engineered construct must elicit a negligible immune reaction in order to prevent it causing an inflammatory response that might reduce healing or cause rejection by the body.
- Biodegradability: The objective of tissue engineering is to allow the body's own cells, over time, to replace the implanted scaffold. Scaffolds and constructs are not intended as permanent implants. Therefore, the scaffold must be biodegradable to allow cells to produce their own extracellular matrix. Also, the products of this degradation should be non-toxic and reabsorbed in the body through a natural via during metabolic processes (bioreabsorbability) or eliminated by means of dissolution.
- Mechanical properties: Ideally, the scaffold should have mechanical properties consistent with the anatomical site into which it is to be implanted.
- Scaffold architecture: As mentioned before, scaffolds should have an interconnected pore structure and high porosity to ensure cell penetration and adequate diffusion of nutrients to cells within the construct and to ECM formed by the cells. Furthermore, a porous interconnected structure is required to allow diffusion of waste products out of the scaffold, and the products of scaffold degradation should be able to exit the body without interference with other organs and surrounding tissues.

- Manufacturing technology: For a particular scaffold or tissue engineered construct to become clinically and commercially viable, it should be cost effective and possible to scale-up.

The final criteria for scaffolds in tissue engineering, which depends on the list above, is the choice of biomaterial from which the scaffold should be fabricated. A wide range of materials including all the classical materials such as metals, ceramics, glasses and polymers have been investigated as biomaterials. Anyway, in the fabrication of scaffolds for tissue engineering three individual groups of biomaterials, ceramics, synthetic polymers and natural polymers, are used.

Numerous synthetic polymers have been used to produce scaffolds. This can be attributed to the inherent flexibility in synthesizing or modifying polymers matching the physical and mechanical properties of various tissues or organs of the body. Furthermore, polymeric scaffolds have unique properties such as high surface-to-volume ratio, high porosity with very small pore size, biodegradation and mechanical properties. On the other hand, they have drawbacks including the risk of rejection due to reduced bioactivity.

Unlike synthetic polymer-based scaffolds, natural polymers are biologically active and typically promote excellent cell adhesion and growth. Furthermore, they are also biodegradable and allow host cells to produce their own ECM and replace the degraded scaffold. However, fabricating scaffolds from biological materials with homogeneous and reproducible structures presents a challenge. In addition, these scaffolds generally have poor mechanical properties which limit their use in some applications [(7)].

The problems described above, which are consequence of using scaffolds fabricated from a single-phase biomaterial, have resulted in considerable research generating the development of composite scaffolds comprising a number of phases. For example, many groups have attempted to introduce ceramics into polymer-based scaffolds or combining synthetic with natural polymers.

2.2.1 Proteins

Proteins are large biomolecules, or macromolecules, consisting of one or more long chains of amino acid residues. Proteins perform a vast array of functions within organisms and they differ from one to another in their sequence of amino acids, which is dictated by the nucleotide sequence of their genes, and which usually results in protein folding into a specific three-dimensional structure that determines its activity. Proteins are natural biodegradable materials and current progress in their applications in tissue engineering have generated considered attention, due to the following reasons [(8)]:

- Proteins have excellent biocompatibility and biodegradability, especially because their degradation products, amino acids, are the basic components of life and can be resorbed as nutrients.

- Some of them induce minimal tissue inflammatory responses.
- Some proteins are available on a large scale and low cost.

Proteins extracted from mammalian tissue can generate a disease transmission as well as batch-to-batch inconsistency. Plant-derived proteins are thus gaining interest for biomedical applications.

Zein is the major storage protein of corn and comprises approximately between 45 and 50% of the protein in corn. Zein has been of scientific interest since its isolation in 1821. Zein belongs to the family of proteins known as prolamines due to their solubility in alcohol-water mixture. Zein defining characteristic is its insolubility in water except in the presence of alcohol, high concentrations of urea, high concentration of alkali (pH = 11 or above) or anionic detergents. This solubility property depends on its amino acid composition, which is characterized by an abundance of hydrophobic and uncharged amino acids as leucine (20%), proline (10%) and alanine (10%) [8]. The high proportion of nonpolar amino acid residues and deficiency in basic and acid amino acids is responsible for the solubility behavior of zein.

Zein is a heterogeneous mixture linked by disulfide bonds. Two major fractions of zein, α and β, were first described by McKinney (1958). α-Zein was defined as the prolamine of corn soluble in 95% ethanol. This protein closely resembles the zein available commercially. β-Zein is soluble in 60% ethanol and insoluble in 95% ethanol. This zein is relatively unstable and consequently was not a constituent of commercial zein preparations [9]. The α-helical proportion of zein amounts to 50-60%, β-sheets comprise about 15%, and the remainder of the molecule is aperiodic.

Wang et al. [8] studied the feasibility of zein as fabricated 3-D porous scaffolds. Zein and its degraded product showed good cell compatibility and did not interrupt the adhesion, growth or proliferation of rat mesenchymal stem cells (MSCs). Porous zein-based scaffolds also showed good mechanical properties.

2.2.2 Synthetic polymers

For tissue engineering applications, many synthetic polymers are blended with proteins in order to improve their biocompatibility and achieve a better cell-material interaction on a molecular level.

2.2.2.1 Polyglycerol sebacate

Polyglycerol sebacate (PGS) is a biodegradable polymer increasingly used in a variety of biomedical applications. This polyester is prepared by polycondensation of glycerol and sebacic acid. Figure 2 shows the PGS chemical structure, where R is a polymer chain. PGS exhibits biocompatibility and biodegradability, both highly relevant properties in biomedical applications. PGS also involves cost effective production with the possibility of scaling to industrial production. In addition, the mechanical

properties and degradation kinetics of PGS can be tailored to match the requirements of intended applications by controlling curing time, curing temperature and reactants concentration [10].

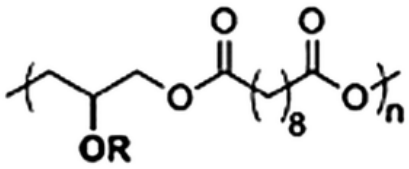

Figure 2. *Chemical structure of polyglycerol sebacate*

PGS is analogous to vulcanized rubber in that it forms a crosslinked, three-dimensional network of random coils (this is the characteristic that is considered to give vulcanized rubber its elasticity). Also, PGS is bioresorbable, it can degrade and further resorb in vivo, with the degradation products eliminated through natural pathways [10].

2.2.2.2 Poly(ε-caprolactone) (PCL)

PCL is an aliphatic polyester obtained by ring opening polymerization of ε-caprolactone. Figure 3 shows its chemical structure. PCL is a semicrystalline polymer and it has been widely used due to its good biocompatibility, easy-processing ability and non-toxic degradation products. The degradation of PCL occurs by hydrolysis of ester bonds into acidic monomers, which can be removed from the body by physiological metabolic pathways.

However, some drawbacks have limited the applications of PCL scaffolds: slow degradation rate, which might be related with its highly crystalline character; hydrophobicity, which is adverse for the cell attachment and penetration into the porous structure; and the acidic degradation products, which might lead to side effects. Blending PCL with natural polymers is an approach to overcome those limitations.

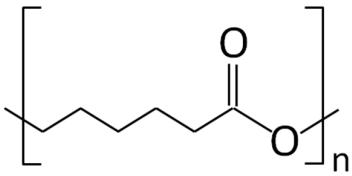

Figure 3. *Chemical structure of PCL*

2.2.3 Nanoscale materials

The application of nanoscale materials is crucial in various approaches to regenerating tissues. Nanotopographical features, when interacting with cells, have been proven to control and regulate

cellular processes as important signaling modalities. Furthermore, nanotopography and local environment influence trends in cell behavior by providing chemical and physical stimuli to promote cell adhesion, proliferation, morphogenesis and motility. The provided stimuli include chemical cues and adsorbed protein motifs, as well as the geometry, dimensions and aspect-ratios of the nanotopographical features.

Nanoscale materials can be fabricated into different forms such as nanoparticles, nanofibers, nanospheres, nanotubes, nanogels, nanocapsules and surfaces with nanotopographical features. These nanostructures can be prepared using a variety of biofabrication methods such as electrospinning, electrospraying, spray drying, phase separation, molecule self-assembly, chemical vapor deposition and nano-imprinting. Among these nanostructures, nanofibers fabricated from electrospinning are one of the most widely investigated platforms for tissue regeneration. They are characterized by ultra-thin continuous fibers, high surface-to-volume ratio, high porosity and adjustable pore size distribution. The highly interconnected porous structure of these scaffolds provides an appropriate substrate for cell attachment and nutrient transport. In addition, the ECM-mimicking nanofibrous structures have been shown to stimulate *in vivo*- like organization and morphogenesis of cells in culture [(11)]. The cells binding to scaffolds with microscale architectures flatten and spread as if cultures on flat surfaces. The scaffolds with nanoscale architecture, on the other hand, have bigger surface area for absorbing proteins and present more binding sites to cell membrane receptors. The adsorbed proteins further can change the conformations exposing additional binding sites, expected to provide an edge over microscale architectures for tissue generation applications.

2.3 Electrospinning technique

Electrospinning has gained popularity in the last 10 years due, in large part, to an increased interest in nanoscale properties and technologies. This technique allows for the production of polymer fibers with diameters varying from 5 nm to 5 μm. The capacity to easily produce materials with this size scale has created renewed interest in electrospinning for applications in tissue engineering and drug delivery. Moreover, the possibility of large scale productions combined with the simplicity of the process makes this technique very attractive for many applications.

The use of electrostatic forces to form synthetic fibers has been known for over 100 years. Figure 4 illustrates the general set-up of an electrospinning apparatus used to create polymeric nanofibers. The apparatus consists of a high-voltage power supply, a solution reservoir (syringe with a needle) and a syringe pump, and a grounded metal collector.

Electrospinning utilizes a high voltage source to inject charge of a certain polarity into a polymer solution or melt, which is then accelerated toward a collector of opposite polarity. As the electrostatic attraction between the oppositely charged liquid and collector and the electrostatic repulsions between like charges in the liquid become stronger, the leading edge of the solution changes from a rounded meniscus to a cone (known as the Taylor cone). A fiber jet is eventually ejected from the Taylor cone as the electric field strength exceeds the surface tension of the liquid. The fiber jet travels through the atmosphere allowing the solvent to evaporate, thus leading to the deposition of solid polymer fibers on the collector [12]. Before reaching the collector, the jet undergoes a series of electrically driven bending instabilities and gradually thins in air due to elongation and solvent evaporation. If the collector is stationary (Fig. 4B), the jet becomes randomly-oriented nanofibers in the form of non-woven web (Fig. 4C). On the other hand, aligned nanofibers can be fabricated by using either a stationary collector with small changes to the collector or different dynamic collectors. In one configuration, shown in Fig. 4D, a rotating drum collector is used at a high speed to obtain aligned nanofibers (Fig. 4E).

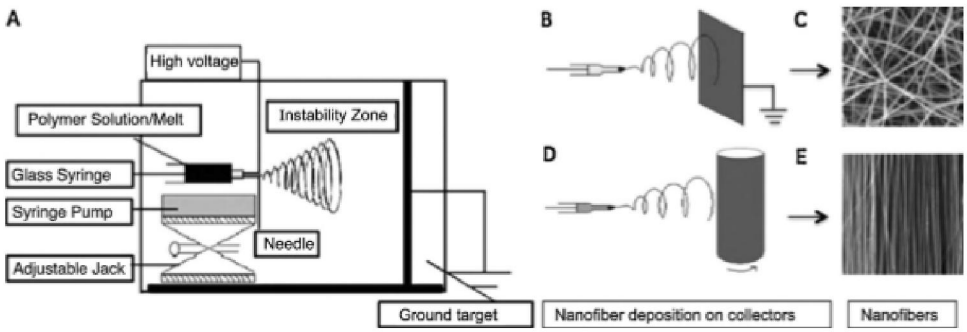

Figure 4. *(A)Schematic diagram of the electrospinning process. (B) A stationary metal collector. (C) Randomly-oriented nanofibers collected on the stationary collector. (D) A rotating drum collector. (E) Uniaxial aligned nanofibers collected on the rotating drum collector.*

2.3.1 Parameters of electrospinning process

The electrospinning process can be manipulated by a number of variables in terms of solution properties, controlled variables and ambient parameters [12]. Solution properties include viscosity, conductivity, surface tension, polymer molecular weight, dipole moment and dielectric constant. The effects of the solution properties can be difficult to isolate since varying one parameter can generally affect other solution properties. Controlled variables include the flow rate, electric field strength,

distance between tip and collector, needle tip design and collector composition and geometry. Ambient parameters include temperature, humidity and air velocity.

While a number of general relationships between processing parameters and fiber morphology can be drawn, it is important to realize that the exact relationship will differ for each polymer/solvent system.

2.3.1.1 Solution parameters

2.3.1.1.1 Viscosity/Concentration

Solution viscosity is controlled by changing the polymer concentration, which determines the spinnability of a solution, whether a fiber forms or not. The solution must have a high enough polymer concentration for chain entanglements to occur; however, the solution cannot be either too dilute or too concentrated. If it is too dilute then the polymer fiber will break up into droplets before reaching the collector due to the effects of surface tension. On the other hand, if the solution is too concentrated then the fibers cannot be formed due to the high viscosity, which makes it difficult to control the solution flow rate through capillary.

In many experiments, it has been shown that within the optimal range of polymer concentration, fiber diameter increases with increasing polymer concentration [(12)].

2.3.1.1.2 Conductivity

Solution conductivity can influence fiber size. Solutions with high conductivity will have a greater charge carrying capacity than solutions with low conductivity. Thus, the fiber jet of highly conductive solutions will be subjected to a greater tensile force in the presence of an electric field than will a fiber jet from a solution with low conductivity. It was shown that, in general, increases in conductivity and charge density produce smaller fibers [(13)]. Furthermore, it has been found that increasing the solution conductivity, through the addition of salt or alcohol to the solvent among others, or charge density can be used to produce more uniform fibers with fewer beads present [(14)].

2.3.1.1.3 Polymer molecular weight

Researchers have found that as the molecular weight increases, the number of beads and droplets is reduced [(11)].

2.3.1.2 Flow rate

In general, it was found that lower flow rates yield fiber with smaller diameters. Flow rates too high results in bending since fibers do not have a chance to dry prior reaching the collector [11].

2.3.1.3 Field strength/Voltage

At low voltages or field strengths, a drop is typically suspended at the needle tip, and a jet will originate from the Taylor cone producing bead-free spinning (assuming that the force of the electric field is sufficient to overcome the surface tension). As the voltage is increased, the volume of the drop at the tip decreases, causing the Taylor to recede. The jet originates from the liquid surface within the tip and more beading is seen. As the voltage is increased further, the jet eventually moves around the edge of the tip with no visible Taylor cone; at these conditions, the presence of many beads can be observed [11].

2.3.1.4 Distance between tip and collector

It has been found that a minimum distance is required to allow the fibers sufficient time to dry before reaching the collector. At distances that are either too close or too far, beading has been observed [11].

2.3.1.5 Ambient parameters

It has been investigated that increasing the temperature yielded fibers with a decreased fiber diameter, and this decline in diameter has been attributed to the decrease in the viscosity of the polymer solutions at increased temperatures [15]. Another study showed that increasing humidity resulted in the appearance of small circular pores on the surface of the fibers and increasing humidity further lead to the pores coalescing [16].

2.3.2 Electrospinning for tissue engineering applications

Compared to self-assembly and phase separation techniques, electrospinning provides a more cost-effective means to produce scaffolds with an interconnected pore structure and fiber diameters in the sub-micron range.

2.3.2.1 Synthetic polymer scaffolds

The most typical method of collecting the electrospun fibers is on a grounded, collecting plate. Because of the randomness of the instable fiber jet, a highly porous, nonwoven fibrous sheet with a large surface-volume ratio is collected. This material is ideal for tissue engineering scaffolds because the high surface area allows for a high percentage of cellular attachment, as well as for multiple focal adhesion

points on different fibers due to nano-sized fiber diameters. Additionally, fibers in the nanometer and submicron range more closely resemble the size scale of extracellular components. Moreover, electrospun nanofiber scaffolds are capable of supporting a wide variety of cell types, they are not only cytocompatible but can also be used to stimulate and encourage cell proliferation and phenotypic behavior [11].

2.3.2.2 Natural polymer scaffolds

Natural polymers are often used because of their enhanced biocompatibility and biofunctional motifs. Compared to synthetic polymers, electrospinning of biological materials is less versatile because a suitable solvent that does not compromise its integrity has to be used. Collagen, alginate, silk, fibrogen, chitosan, among others have been electrospun for biomedical applications [11].

2.3.2.3 Composite scaffolds

Composite scaffolds can also be created using electrospinning. For example, by sequentially spinning different polymer solutions, a scaffold with layers can be created. Each layer can be tailored for specific cell adhesion. Alternatively, two or more polymer solutions can be spun concurrently resulting in a scaffold with mixed types of fibers. A strategy is to use a polymer that degrades faster than other, thereby increasing the microvoid spaces for tissue in-growth [11]. Further, composites can be created with the use of inorganic and organic phases. For example, polymers can be electrospun with ceramics (like hydroxyapatite and bioactive glasses particles)

3. Objectives

The main objectives of this work are:

- To fabricate electrospun zein-based fibrous scaffolds by using benign solvents for the electrospinning process.
- To optimize processing parameters for the production of electrospun zein-based scaffolds
- To investigate the use of non-toxic crosslinker agents for zein to enhance the water stability and cytocompatibility of zein electrospun fibers.
- To determine the mechanical properties of the obtained zein-based electrospun mats.
- To characterize the scaffolds by SEM and FTIR techniques.
- To investigate the degradation behavior of zein electrospun fibers.

4. Materials

Zein and two synthetic polymers, poly (ε-caprolactone) (PCL) and poly (glycerol sebacate) (PGS) were used. Citric, acetic and formic acid were used as crosslinker agents. All materials and reagents were purchased from Sigma Aldrich, Germany with the exception of PGS, which was synthetized in the lab during my stay at FAU, Erlangen, Germany. The polymer synthesis was carried out in two steps:

(1) Pre polycondensation step.

(2) Crosslinking.

For the polycondensation process, equimolar mixtures (1 M) of glycerol and sebacic acid (14.6 ml of glycerol and 40.4 g of sebacic acid) were reacted at 120 °C under nitrogen for 24 h. The resulting non-crosslinked pre-polymer is then further cured for several days at the same temperature as in the first step but under vacuum to remove the water by-product.

Ethanol was used as solvent for non-crosslinked samples and phosphate buffer saline (PBS) was used as medium during degradation tests (pH=7.4).

From now on, the samples will be mentioned as follows:

Zein E: Zein non-crosslinked (with ethanol as solvent)

Zein AA: Zein non-crosslinked (with acetic acid as solvent)

Zein/PGS: Zein/PGS blend

Zein/PCL: Zein/PCL blend

5. Methods

5.1 Fabrication of electrospun scaffolds

Four types of nanofibrous mats were prepared using electrospinning technique: crosslinked and non-crosslinked zein mats, and blends of zein/PCL and zein/PGS.

For the preparation of crosslinked zein samples, the procedure reported by Jiang et al. was followed [17]. A solution of 70 wt% ethanol was prepared. Then, citric acid was dissolved in this solution to obtain a 9 wt% citric acid solution. The effect of citric acid crosslinking was enhanced by increasing the pH of the citric acid solutions. Therefore, the pH of the crosslinking solution was adjusted to 4.9 by adding sodium hydroxide solution (in 70% ethanol, 0.125 g/ml). It was not possible to obtain a crosslinking solution with a higher pH because phase separation occurred when more sodium hydroxide solution was added.

Zein solutions (50 wt.%) were prepared by dissolving zein powder in the pH adjusted citric acid solution. Pre-crosslinking was performed by ageing the zein solutions in sealed containers for 48 h at room temperature, in order to allow expansion of zein molecular chains and formation of crosslinks. After pre-crosslinking the concentrations of pre-crosslinked zein stock solutions were diluted from 50 to 26 wt.% with 70 wt.% ethanol in order to obtain the zein solutions for electrospinning.

The electrospinning was carried out at a flow rate of 0.96 ml/h with an applied voltage of 15 and 19.5 kV. The needle-tip to aluminum collector distance was maintained at 20 cm. The electrospun zein mats were post-crosslinked by heating the electrospun mats at 150 °C for 2.5 h in an oven.

Uncrosslinked electrospun zein mats were also prepared to use as control using the same procedure except adding citric acid (Zein E sample). The processing parameters used for electrospinning were the same.

In addition, zein solutions of 30 wt.% with acetic acid were also prepared (Zein AA). In this case, the electrospinning was carried out at a flow rate of 0.31 ml/h with an applied voltage of 15 kV and a needle-tip to collector distance of 15 cm.

For the blend zein/PGS, solution was obtained by adding PGS 5 wt.% to 20 ml of acetic acid. It was stirred overnight and then zein 30 wt.% was added. The electrospinning was conducted at a flow rate of 0.61 ml/h, a voltage of 15 kV and distance between the tip of the syringe and the collector of 15 cm.

For the zein/PCL blend, two types of samples were prepared. One used acetic and formic acid as crosslinker agents and the other one only acetic acid (named as Zein/PCL). In the first type, a solution of 5 ml of acetic acid and 5 ml of formic acid was prepared. PCL 15 wt.% was added to the solution, and the solution was stirred until a homogeneous solution was obtained. Then, the same amount of zein was added. Electrospinning was carried out at a flow rate of 0.31 ml/h with an applied voltage of 15 kV. The distance between the tip of the needle and the aluminum foil was 15 cm.

In the second case, PCL 20 wt.% was added to a solution of 10 ml of acetic acid and then zein 10 wt.% was added. The flow rate was 0.54 ml/h. The voltage and the distance between syringe needle and collector used for electrospinning were the same as in the first case.

Figure 5 shows the electrospinning equipment used in this project. A plastic syringe and a stainless-steel needle with 21 cm internal diameter were used.

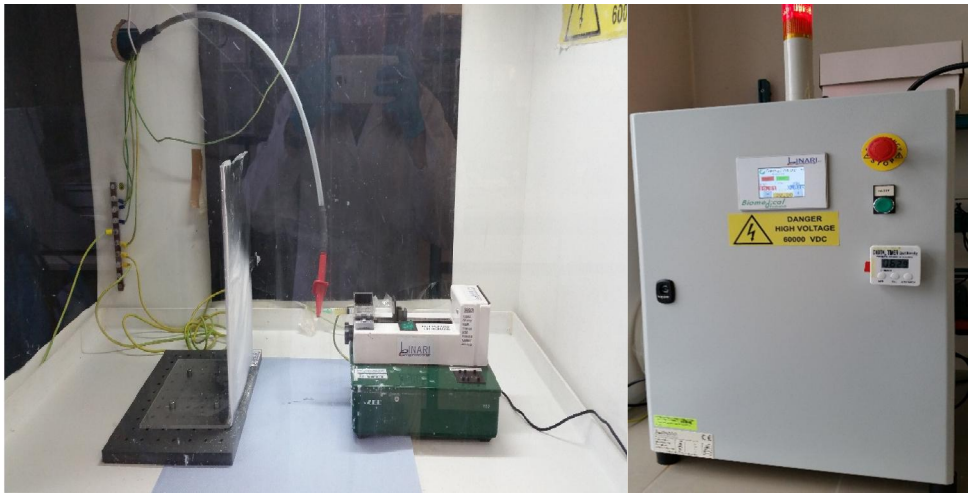

Figure 5. *Digital images of the electrospinning equipment, Starter Kit 40KV Web, used in this work purchased by Linari srl (Italy) available at the facilities of Institute of Biomaterials (Erlangen, Germany)*

All the electrospun parameters are shown in Tables 1 and 2. Table 1 indicates the electrospinning process parameters while Table 2 shows the post-processing conditions. The variations in temperature and humidity among samples can affect the obtained results.

Table 1:

Polymer	**Solvent**	**Solution concentration**	**T (°C)**	**RH**	**Voltage (kV)**	**Distance (cm)**	**Flow rate (ml/h)**
Zein C	Citric acid+ Ethanol	26 wt%	23.6	42%	15.0	20	2.5
Zein	Ethanol	26 wt%	23.3	41%	19.5	20	2.5
Zein	Ethanol	26 wt%	23.5	30%	19.5	20	2.5
Zein E	Ethanol	26 wt%	23.5	33%	19.5	20	2.5

Zein C	Citric acid+ Ethanol	26 wt%	23.9	32%	19.5	20	2.5
Zein AA	Acetic acid	30 wt%	23.5	48%	15.0	15	0.8
Zein/PCL	Acetic acid+Formic acid	15 wt.% Zein and 15 wt.% PCL	23.3	50%	15.0	15	0.8
Zein/PGS	Acetic acid	5 wt.% PGS and 30 wt.% Zein	23.5	31%	15.0	15	1.6
Zein/PCL	Acetic acid	20 wt.% PCL and 10 wt.% Zein	23.9	30%	15.0	15	1.4
Zein	Acetic acid	30 wt%	23.5	27%	15.0	15	0.8
Zein/PCL	Acetic acid	20 wt.% PCL and 10 wt.% Zein	23.8	28%	15.0	15	1.4
Zein/PCL	Acetic acid	20 wt.% PCL and 10 wt.% Zein	23.3	28%	15.0	15	1.4
Zein/PCL	Acetic acid	20 wt.% PCL and 10 wt.% Zein	24.0	33%	15.0	15	1.4

Table 1. *Details of electrospinning process parameters*

Polymer	**Solvent**	**Solution concentration**	**Time**	**T (°C)**	**RH**
Zein C	Citric acid+ Ethanol	26 wt%	1 h 52 min	23.9	44%
Zein	Ethanol	26 wt%			
Zein	Ethanol	26 wt%	2 hs 5 min	23.5	30%
Zein E	Ethanol	26 wt%	4 hs	23.9	36%
Zein C	Citric acid+ Ethanol	26 wt%	4 hs	24.3	33%
Zein AA	Acetic acid	30 wt%	2 hs	23.3	49%
Zein/PCL	Acetic acid+Formic acid	15 % (w/v) Zein and 15 % (w/v) PCL	2 hs	23.1	50%
Zein/PGS	Acetic acid	5 wt.% PGS and 30 wt.% Zein	3 hs 35 min	23.9	31%
Zein/PCL	Acetic acid	20 wt.% PCL and 10 wt.% Zein	2 hs	23.9	30%
Zein	Acetic acid	30 wt%	4 hs	23.6	26%
Zein/PCL	Acetic acid	20 wt.% PCL and 10 wt.% Zein	2 hs 15 min	24.0	28%
Zein/PCL	Acetic acid	20 wt.% PCL and 10 wt.% Zein	2 hs	23.6	30%
Zein/PCL	Acetic acid	20 wt.% PCL and 10 wt.% Zein	2 hs	23.8	33%

Table 2. *Post-processing conditions of electrospinning*

Samples marked in bold font were used for studies carried out in this project.

5.2 Degradation test

Degradation tests was conducted in PBS for 28 days at body temperature (37°C) using the procedure reported by Dippold et al. [18]. Weight loss, water uptake, pH and temperature changes were recorded at different period of time (1, 7, 14, 21 and 28 days). Three specimens were tested for each degradation time. The specimens were taken off the aluminum foil and rectangular pieces (40x10 mm^2)

of were cut. The initial mass of each one was measured before they were separately placed in capped plastic bottles containing 10 ml of PBS solution, as can be seen in Figure 6. Samples were placed in an incubator (KS 4000 I Control (IKA, Germany)) at 37°C with mild shaking (90 rpm) for the specified incubation times. When the testing time was over, the pH and temperature were measured using a Jenway 3510 pH meter (Bibby Scientific limited, UK). Samples were then removed from the PBS solution, washed with deionized water and dried with tissue paper. The mass of each specimen was then recorded ("wet mass"). After being weighed, the samples were then dried for a period of 72 hours and were weighed again ("dry mass").

The weight loss was calculated using the following equation:

$$\%\ weight\ loss = \frac{m_i - m_d}{m_i} x100 \quad \text{(Equation 1)}$$

And the water uptake was calculated with:

$$\%\ water\ uptake = \frac{m_w - m_i}{m_i} x100 \quad \text{(Equation 2)}$$

Where m_i is the initial mass of the specimens, m_d is the dry mass after 72 h and m_w is the wet mass of the samples after taking them out of the PBS solution.

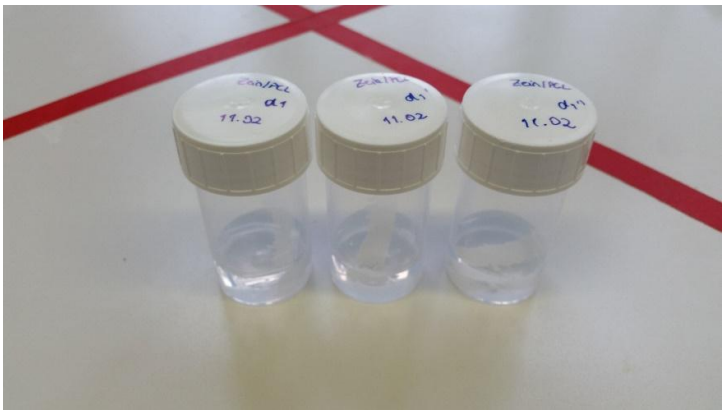

Figure 6. *Plastic bottles containing PBS and the samples*

5.3 Microstructural and morphological characterization

5.3.1 Fourier transform infrared spectroscopy (FTIR)

Infrared analysis of the samples was carried out using an FTIR spectrometer (Nicolet 6700, Thermo Scientific Germany) with attenuated total reflectance mode (ATR). This technique allows the identification of the presence of characteristic functional groups of the surface of a material. For the

analysis, 32 scans with a resolution of 4 cm^{-1} and a wave length in the range of 4000-550 cm^{-1} were performed. The window material was CsI. Samples were analyzed before and after the degradation test.

Since some samples, especially after the degradation test, were too brittle, it was necessary to prepare discs applying a pressure of 10^5 N using an electro hydraulic press (Elektro-Hydraulische Press mit Werkzeug, FAU, Germany), as shown in Figure 7. For this, 2 mg of the samples were milled and mixed with 0.2 g of potassium bromide (KBr). A KBr disc was also prepared for calibration purposes. The resulting discs are shown in Figure 8.

Figure 7. *Image of the equipment used to make discs for FTIR analysis*

Figure 8. *Example of the disc of Zein/PGS sample and KBr*

5.3.2 Scanning electron microscopy (SEM)

Samples were examined by SEM for morphology evaluation. A FE-SEM-EDS microscope (Auriga 0750, Zeiss, Jena, Germany) was used. Samples were sputtered with gold before SEM analysis using a Sputter Coater (Q150T, Quorum Technologies, Darmstadt, Germany). Samples were analyzed before and after the degradation test.

Moreover, SEM micrographs were analyzed to determine the mean diameter and diameter distribution of the fibers. An amount of 100 fibers per image were measured using Image ProPlus software.

5.4 Mechanical test

Uniaxial tensile tests of the samples before and after the degradation test were performed. Zein AA, Zein/PGS and Zein/PCL were analyzed before the degradation test. The tensile test of Zein E was not performed due to its very low strength. Regarding the samples after the degradation test, only Zein/PCL after 1, 7 and 14 days of incubation were tested. Three samples of each composition were tested.

Samples were taken off the aluminum foil and specimens of 30 mm length and 5 mm width were cut. The thickness was measured with a micrometer. In the case of samples before degradation test, a paper frame was prepared for each sample, as shown in Figure 9. After degradation, samples were mounted in a plastic frame to place sample and frame in PBS medium (Figure 10). Otherwise, it was difficult to prepare the settings with the degraded samples. The frames were cut in the middle to ensure that the tensile strength was measured only on the fibers rather than the frames.

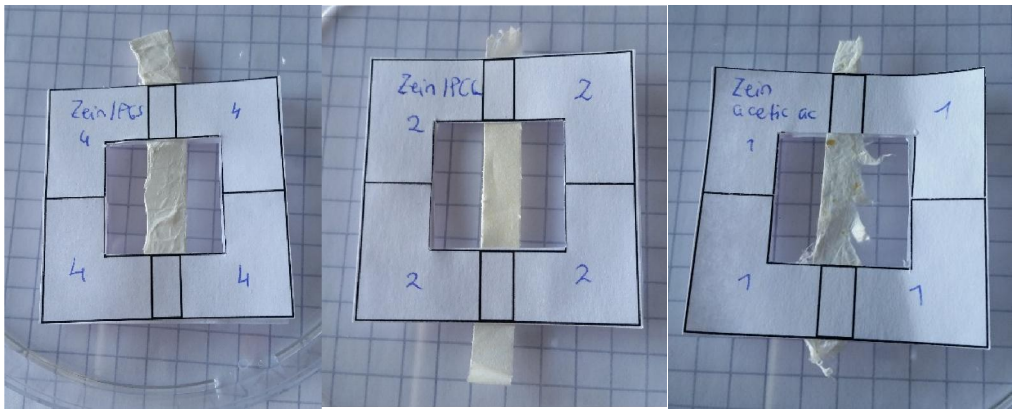

Figure 9. *Samples prepared for tensile test (before degradation)*

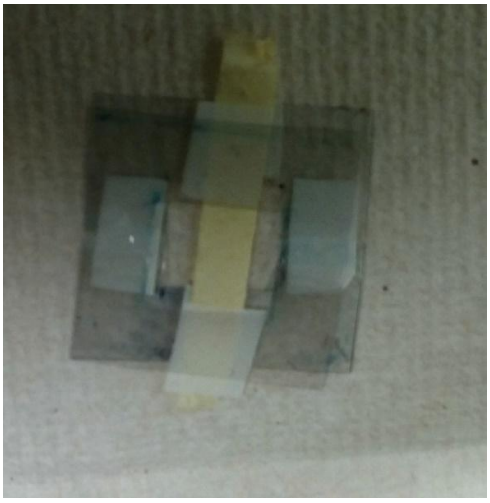

Figure 10. *Zein/PCL sample prepared for tensile test (after degradation)*

The mechanical properties of the scaffolds were tested with a universal testing machine Zugfestigkeitsprüfmaschine Frank, K. Frank GmbH, Mannheim, Germany, as showed in Figure 11. A load cell of 50 N and a crosshead speed of 10 mm/min were used.

Figure 11. *Tensile test machine during the test*

6. Results and discussion

6.1 Fabrication of electrospun mats

Figure 12 (A-D) displays SEM images of the samples before degradation test. SEM micrograph of Zein E (Figure 12 A) shows uniform bead-free nanofibers with a flat morphology rather than rounded nanofibers. Zein AA mats shows bead-free rounded nanofibers (Figure 12 B). Zein/PGS (Figure 12 C) presents fiber morphology similar to Zein AA. Zein/PCL blend (Figure 12 D) present a complex morphology, known as nanoweb or "net in the net" morphology, where tiny polymer strands fill the gaps between larger fibers. Therefore, clear differences between the different mixtures were observed.

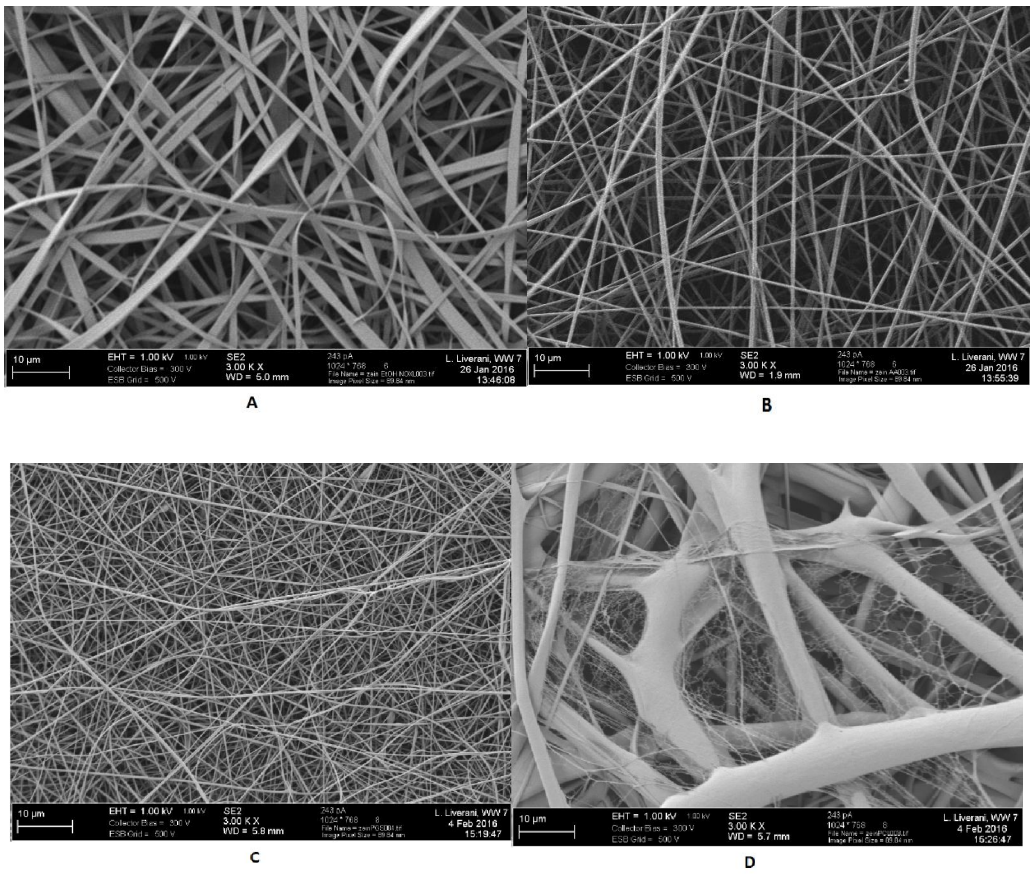

Figure 12. *SEM images of the samples. (A) Zein E. (B) Zein AA. (C) Zein/PGS. (D) Zein/PCL*

Table 3 and Figure 13 show the mean diameter and standard distribution (s.d.). A detailed evaluation of the images revealed that the change of the solvent used in the electrospinning process had an important effect in fiber size. Zein AA exhibited a decrease in fiber diameter with respect to Zein E. Moreover, the lowest fiber diameter was obtained for Zein/PGS blend. Due to the complex morphology

of Zein/PCL samples only larger fibers were measured. Among these fibers, two populations (fibers < 2 μm and fibers > 2 μm) were measured.

Sample	Fiber size (μm)
Zein E	1.8±0.5
Zein AA	0.8±0.2
Zein/PGS	0.4±0.1
Zein/PCL 1	4±2
Zein/PCL 2	1.2±0.3

Table 3. *Fiber diameters of the studied samples*

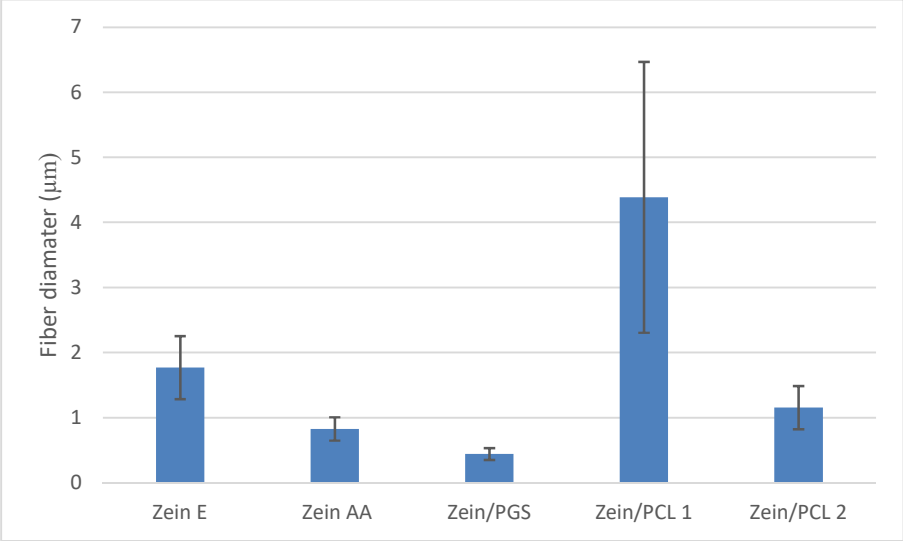

Figure 13. *Fiber diameter distribution of the studied samples*

Figure 14 shows the SEM micrograph of Zein E after one and seven days of degradation. It can be observed that after one day the nanofiber morphology is completely lost, evidencing a fast degradation of the sample and the need of crosslinking to enhance the sample stability.

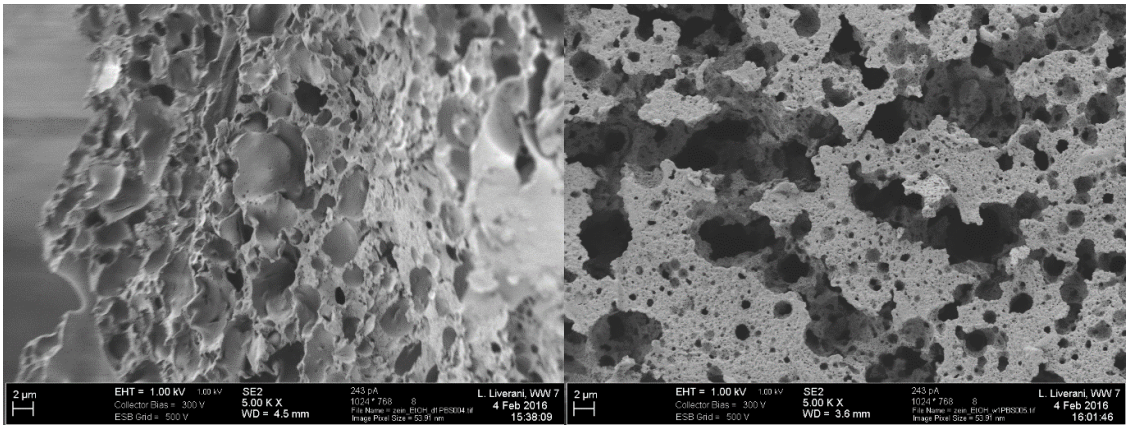

Figure 14. *SEM micrograph of Zein E after degradation. Left: One day of degradation. Right: One of degradation.*

Figure 15 shows a similar behavior for Zein AA than Zein E. It is evident that after one day in PBS medium, the fibers are totally degraded. After seven days of degradation, probably a contamination of the sample occurred, showing the morphology reported in the right part of Figure B.

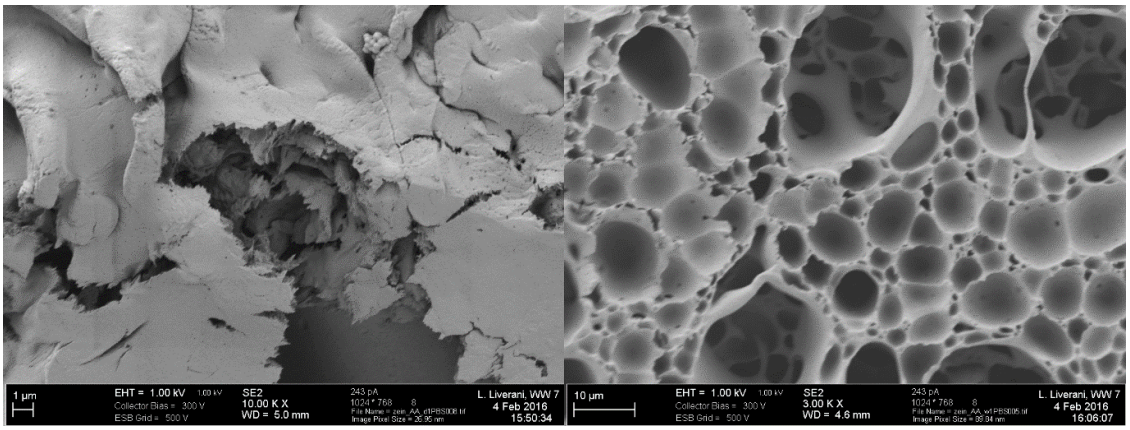

Figure 15. *SEM micrograph of Zein AA after degradation. Left: One day of degradation. Right: One week of degradation.*

For Zein/PGS the same result as the two cases before were observed (Figure 16).

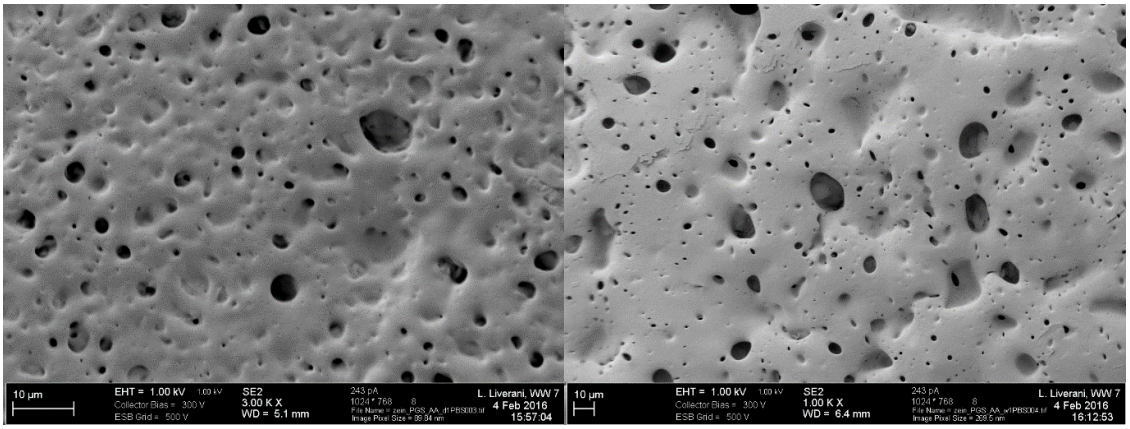

Figure 16. *SEM micrograph of Zein/PGS after degradation. Left: One day of degradation. Right: One week of degradation.*

Sample Zein/PCL exhibited a different behavior, as can be seen in the following figures. In Figure 17, SEM micrographs of the sample after one day of degradation is shown. Here it is evident that the nanofibers did not degrade but they show a little distortion and the nets between the fiber disappeared. Pure PCL degrades by hydrolysis in some months or years, depending on the sample morphology, and can delay the degradation process when is blended with other polymer.

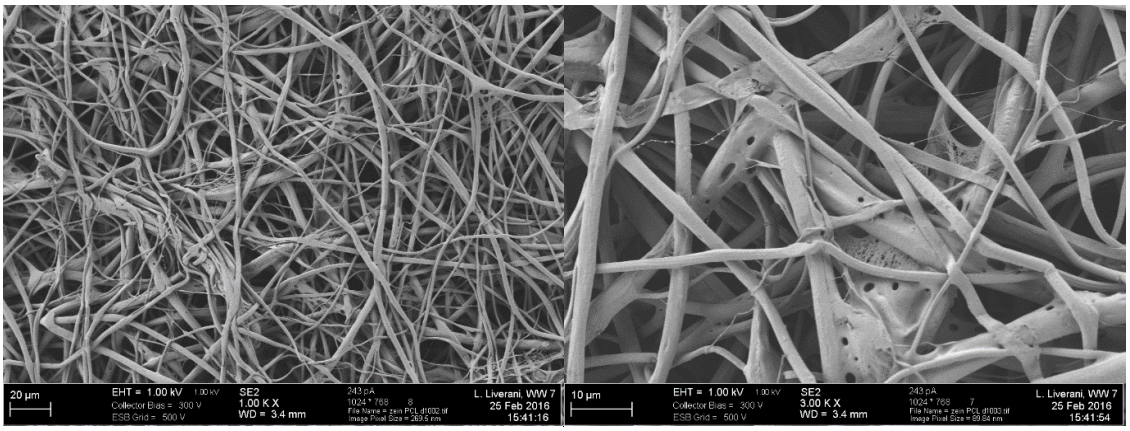

Figure 17. *SEM micrograph of Zein/PCL after one day of degradation*

Figure 18 shows the SEM images after seven days of incubation. In this case the fibers are more degraded than before, they are cut and deformed.

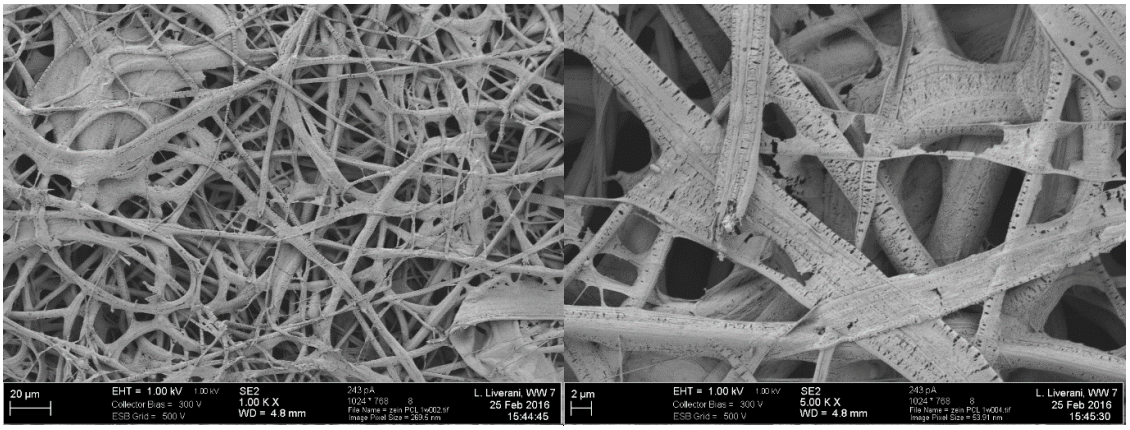

Figure 18. *SEM micrograph of Zein/PCL after one week of degradation*

In Figure 19 SEM micrographs of sample Zein/PCL after two weeks of degradation are displayed. In these images it is also evident the progression of the nanofiber degradation, although it does not differ too much from the sample after one week of degradation.

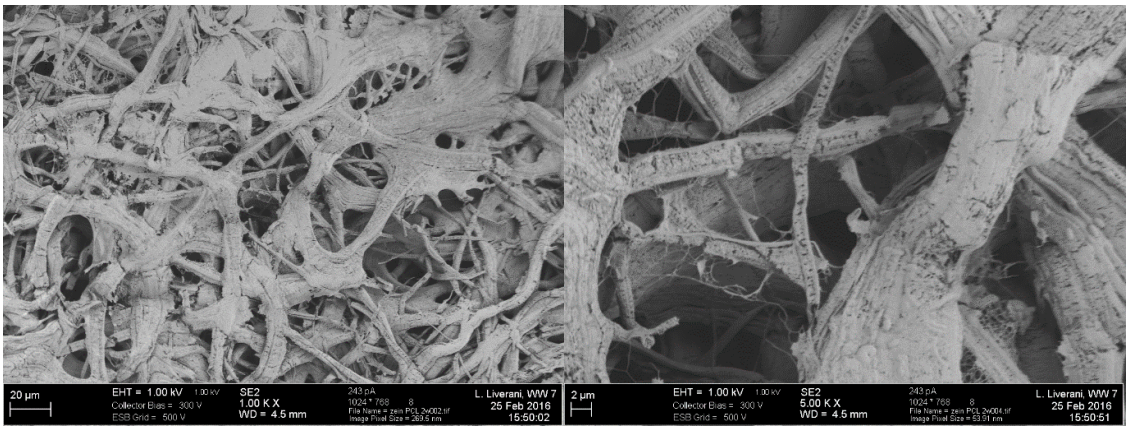

Figure 19. *SEM micrograph of Zein/PCL after two weeks of degradation*

Figure 20 shows SEM micrographs of Zein/PCL after three weeks of degradation. It can be noticed that there are still nanowebs, probably composed of PCL.

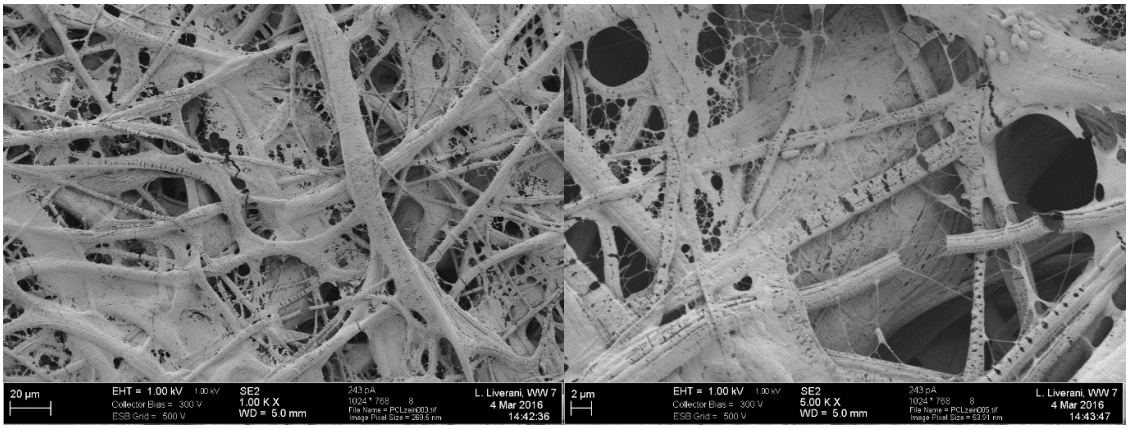

Figure 20. *SEM micrograph of Zein/PCL after three weeks of degradation*

In Figure 21 micrographs corresponding to four weeks of degradation are shown. This sample appears less degraded than the samples with shorted incubation times. Therefore, based on these images a clear correlation cannot be established.

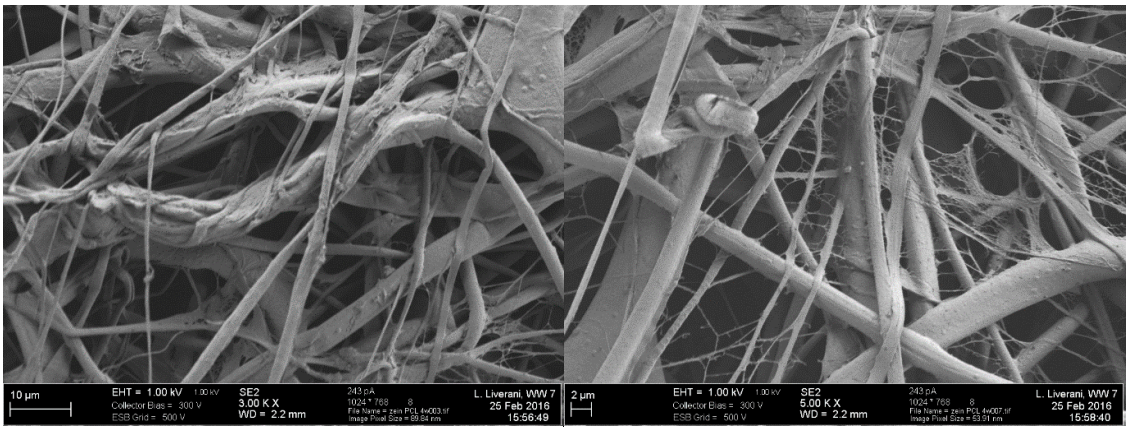

Figure 21. *SEM micrograph of Zein/PCL after four weeks of degradation*

6.2 Degradation behavior

The degradation of the zein-based mats was studied *in vitro.* Figure 22 shows the samples after one day of degradation when they were completely dried. Comparing the samples, Zein/PCL was the one which resulted more intact and Zein AA suffered the greatest damage. Zein/PGS ended up not as good as Zein/PCL but survived better the test than Zein E and Zein AA. These results evidence that blending zein with a synthetic polymer improves the degradation behavior.

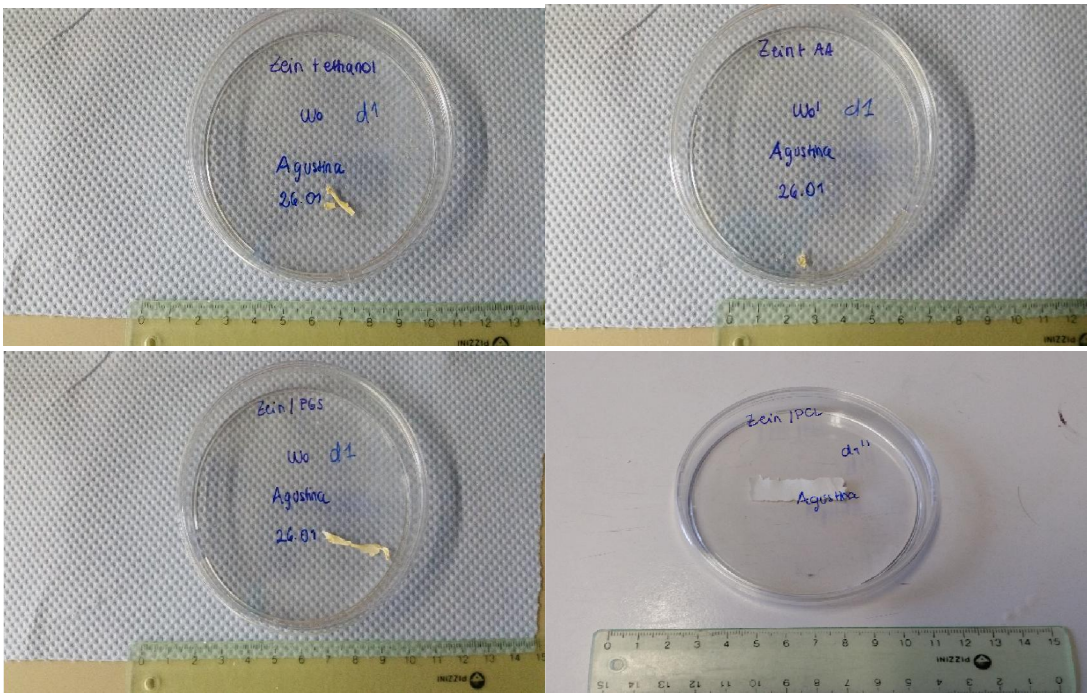

Figure 22. *Samples after one day of degradation*

Figure 23 displays the images of samples after one week in PBS medium. As in the previous case, Zein/PGS and Zein/PCL showed more stability to degradation than Zein E and Zein AA.

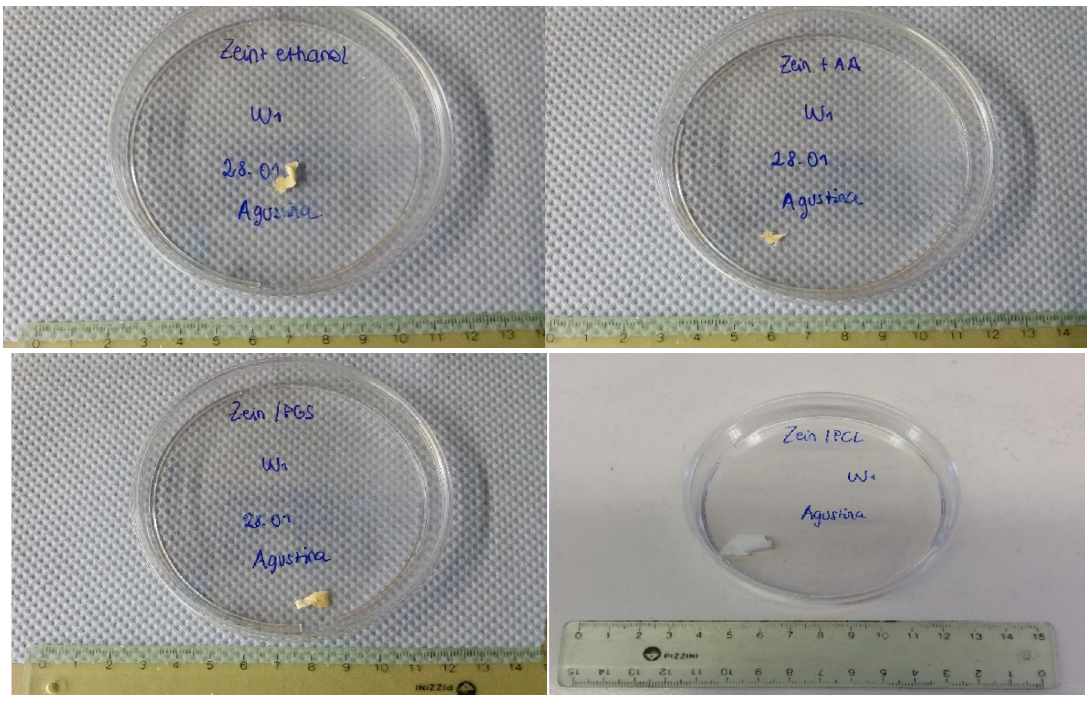

Figure 23. *Samples after one week of test*

Figure 24 shows the samples after 14 days of test. After this incubation time Zein/PCL still has the lowest damage followed by Zein/PGS. This is in agreement with the blending with a synthetic polymer.

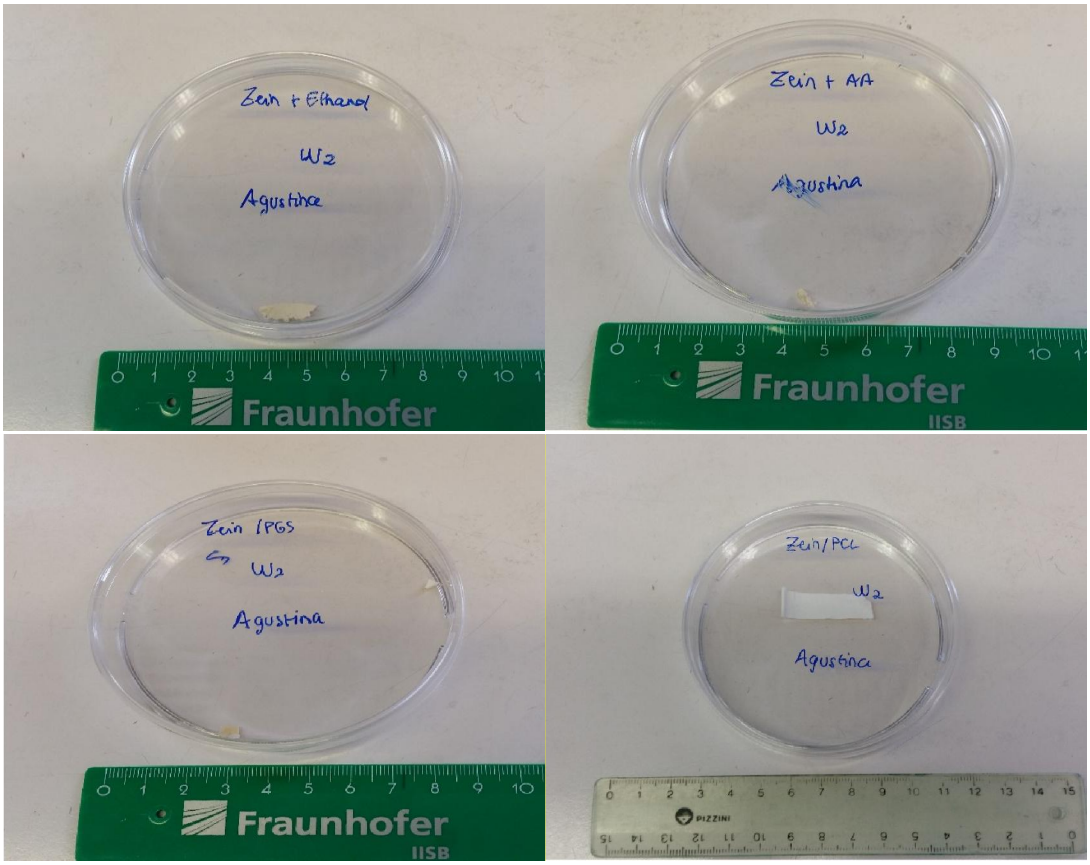

Figure 24. *Samples after two weeks of test*

Figure 25 shows the samples for three weeks of incubation time. After this period, none of the three samples of Zein E survived. Regarding Zein AA, the sample was almost completely degraded. Zein/PGS resulted more degraded than Zein/PCL, which remained almost intact.

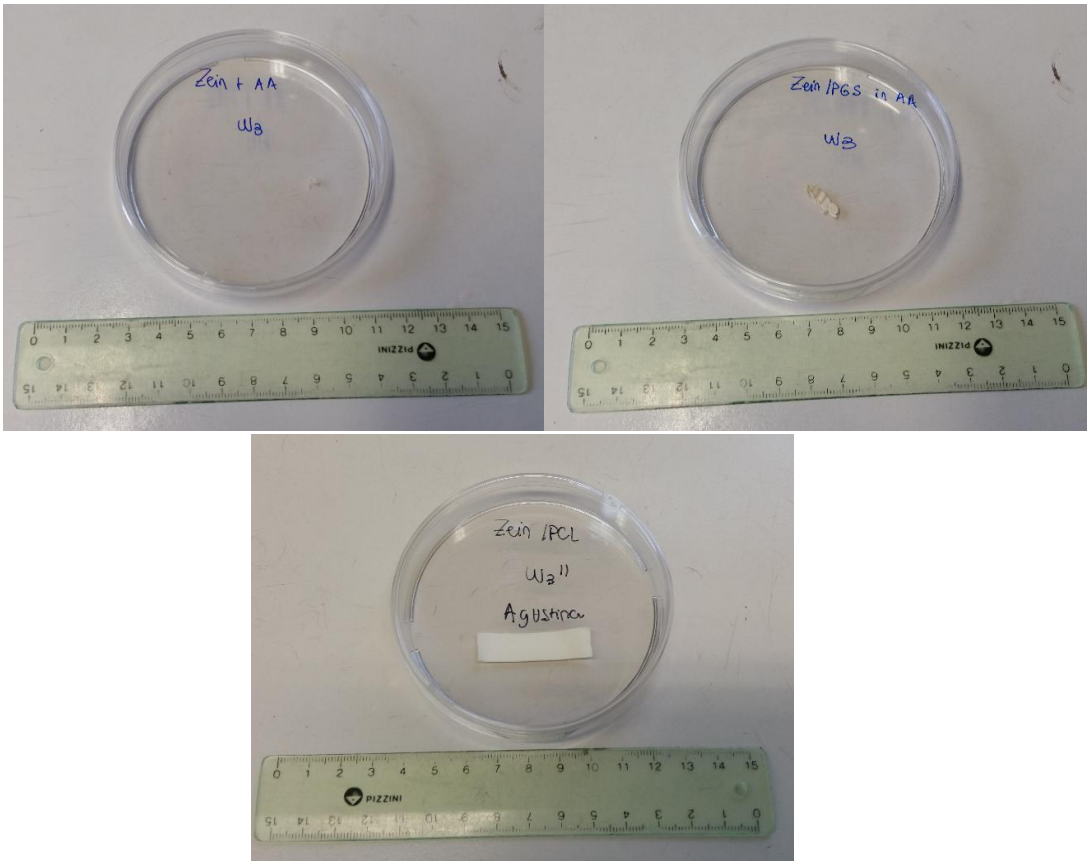

Figure 25. *Samples after three weeks of test*

Samples after four weeks degradation are shown in Figure 26. Surprisingly, the four samples survived the test. The difference in the observed behavior for Zein E samples could be attributed to small differences in samples thickness or other non-established causes. Other than that, the performance of the samples followed the same trend as the previous periods of time.

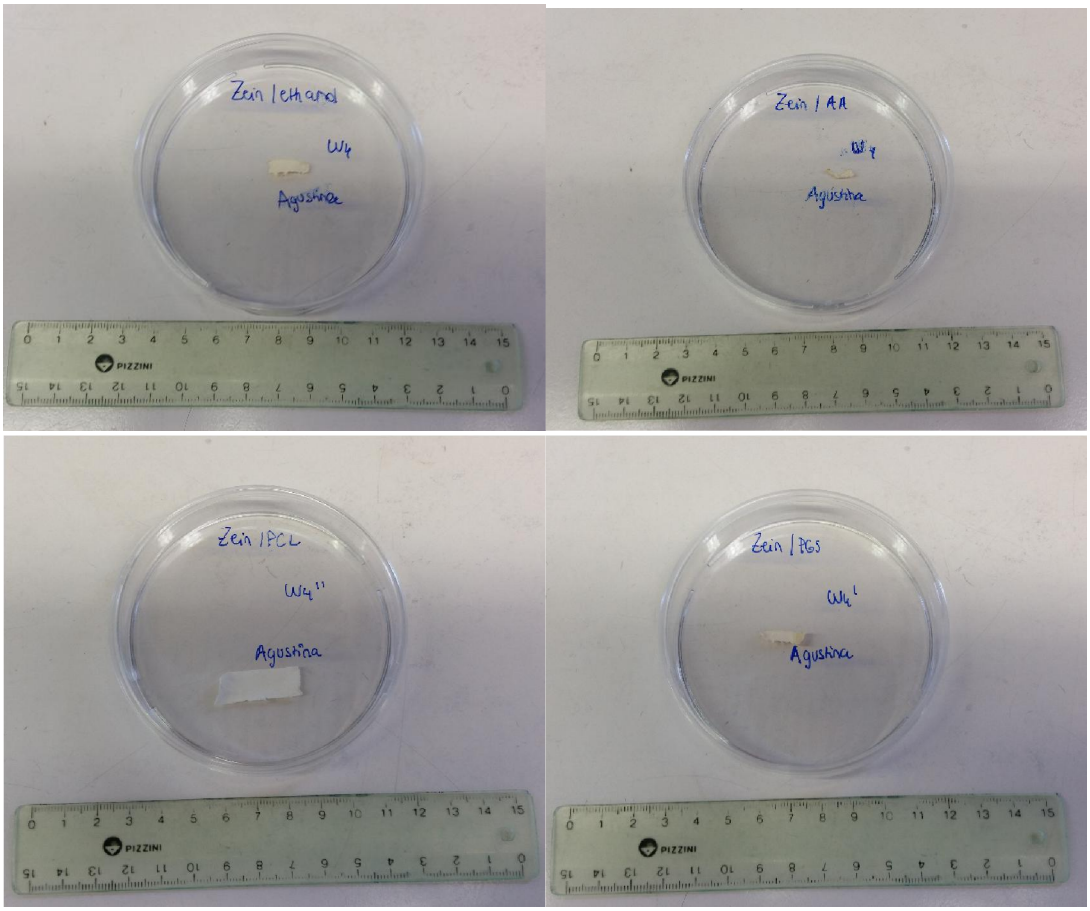

Figure 26. *Samples after four weeks of test*

In vivo studies reported the important effect of pore size on scaffolds degradation, which is due to enhancement of the functions of specific cells by specific pore sizes, consequently leading to more protease secretion. The degradation rate of protein scaffolds could also be influenced by the factors affecting cell functions, such as pore-interconnectivity and surface morphology. There are other factors affecting the degradation of the scaffolds, such as inhibitors or promoters to proteases, cross-linking between protein molecules, processing conditions and the biocompatibility. [(19)]

In this work, *in vitro* degradation was only studied in terms of weight loss and water uptake. But these results also show the importance of pore size, pore-interconnectivity and surface morphology. In Figures 27 and 28, it can be seen water uptake and weight loss as a function of incubation time for the four samples studied. The dispersion in the obtained values was higher than the expected. Small variations in sample thickness and environmental conditions among different samples could be the reason of such dispersion. In the case of testing only one sample, error bars are not displayed.

Water uptake capability is an important parameter for tissue engineering scaffolds as it can give a hint on water absorption and diffusion characteristics which are of major importance to enable cell integration and to ensure nutrition and blood supply during cell growth and proliferation. [18]

It can be seen in Figure 27 that the amount of water absorbance is significantly higher for Zein/PGS and Zein/PCL than Zein E and Zein AA. Although PCL is a hydrophobic polymer, water uptake is related to the surface of the sample and it could have happened that the surface had more zein than PCL leading to a higher water absorbance than expected.

Water uptake by a material can occur by way of "absorbed water", meaning the water absorbed from the media into the material, which depends mainly on the hydrophilicity of the material. Nevertheless, capillary water is the water that is "drawn in" through pores or capillaries of the material. The amount of water absorbed into a scaffold is related to the scaffold porosity and the amount of water available at the surface of the material. For this reason, a porous material can take up and store more water whereas its non-porous (dense) counterpart can store only a limited amount of water [20]. So, in this case, if Zein/PCL sample had more zein on the surface and major porosity than the other samples, due to the "net in the net" morphology, it could lead to a greater water uptake. Regarding Zein/PGS, pure PGS shows a limited water uptake capacity [21], but results show that this is improved many folds by the addition of natural zein protein.

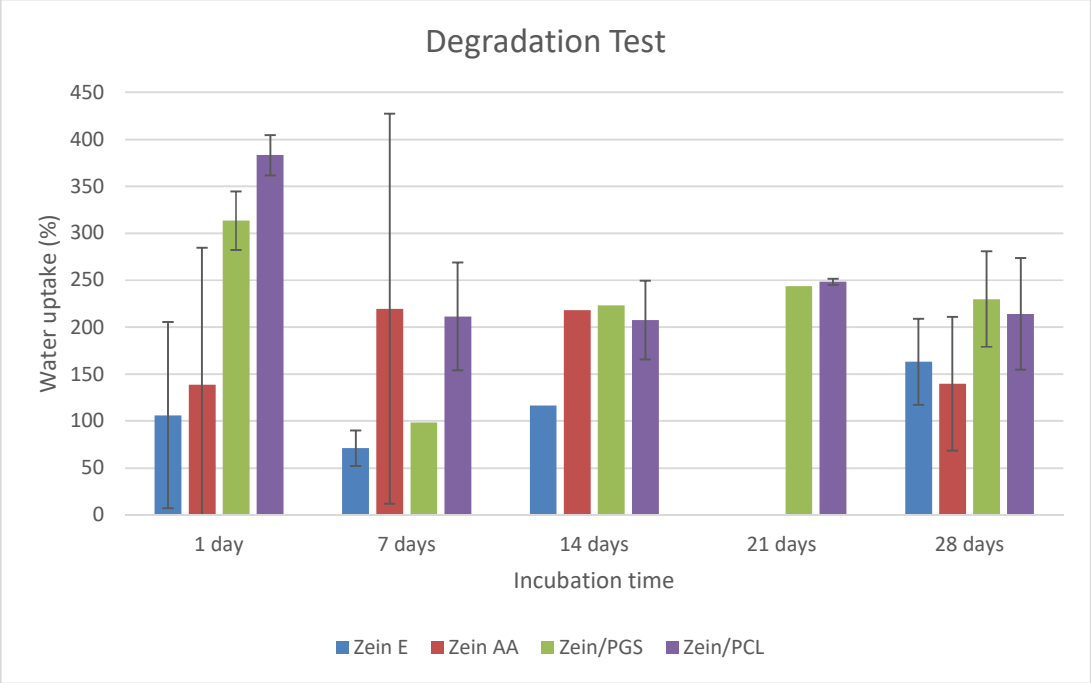

Figure 27. *Water uptake vs. incubation time*

The predicted weight loss graph should show an increase of the weight loss with increasing incubation time, but this was not obtained. Instead, there is not a general tendency in the results. The

samples became very brittle and instable over time and were difficult to measure, which probably led to the large deviation. The major weight loss is attributed to Zein AA at 21 days with 85%. These results correspond to the previous images confirming that the weight loss of Zein/PGS and Zein/PCL is less, in general, than Zein E and Zein AA.

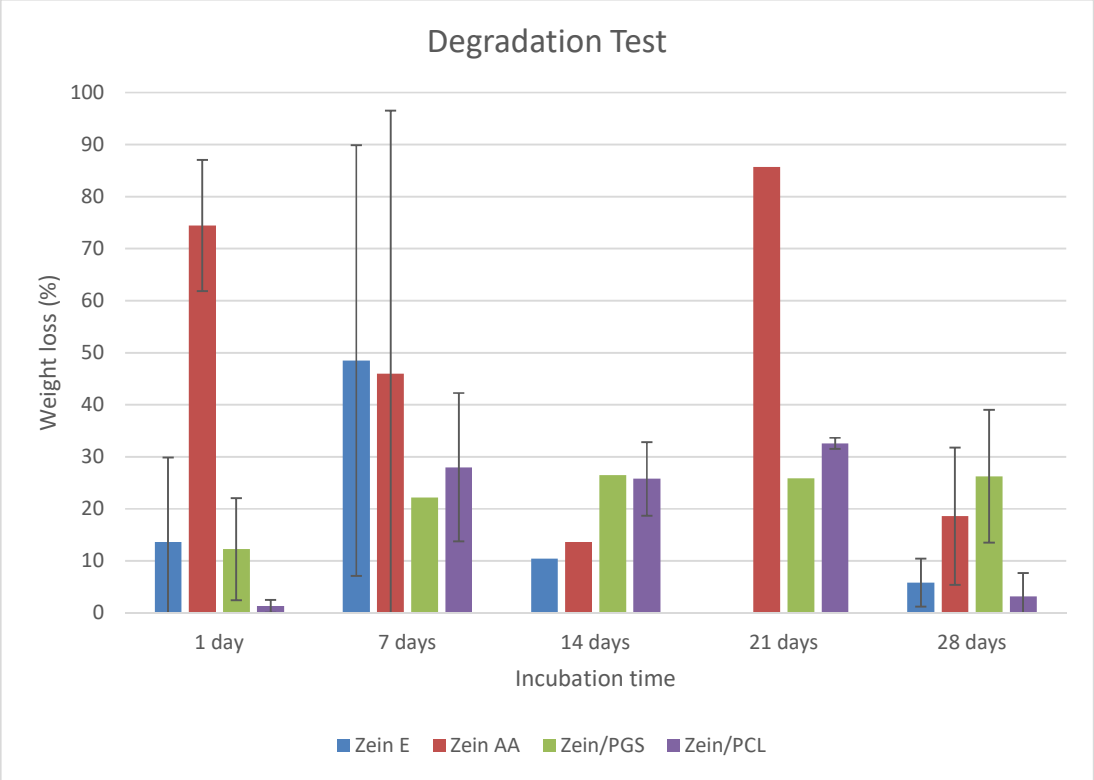

Figure 28. *Weight loss vs. incubation time*

The pH profile can be seen in Figure 29. The pH of the PBS medium before sample immersion was 7.52. Zein likely reacts via hydrolysis with the PBS solution and zein fragments are released from the fibers during incubation time in PBS. The pH of pure zein varies depending on its amino acid composition but generally it lies in the alkaline range [22]. For this reason, the release of zein fragments should cause the increase of pH. The pH takes its highest value in the first week of degradation and it is higher for Zein AA.

At the beginning, the four samples show a drop in the pH. However, between 1 and 7 days of incubation, there is an increase in the pH of Zein E, Zein AA and Zein/PGS which was expected according to the release of zein. After 7 days, another decrease in pH values appears which continues

until 21 days for Zein AA and Zein/PGS while the pH of Zein E increases again after 2 weeks of degradation.

Regarding Zein/PCL, the behavior is lightly different from the other samples. There is a decrease in the pH during the first two weeks of degradation but afterwards it was detected an increase in pH values. In this case, the acidification of the PBS is higher due to acidic products of the polymer degradation.

On the other hand, the degradation of PGS after one week shows a constant slowly decreasing pH due to the presence of unreacted carboxylic acid groups of the PGS backbone as well as their release during the hydrolysis of ester linkages during degradation. Anyway, the difference of pH of the samples in each incubation time is not so sharp.

The pH of the samples was stabilized after 21 days and the final pH was between 7.3 and 7.5.

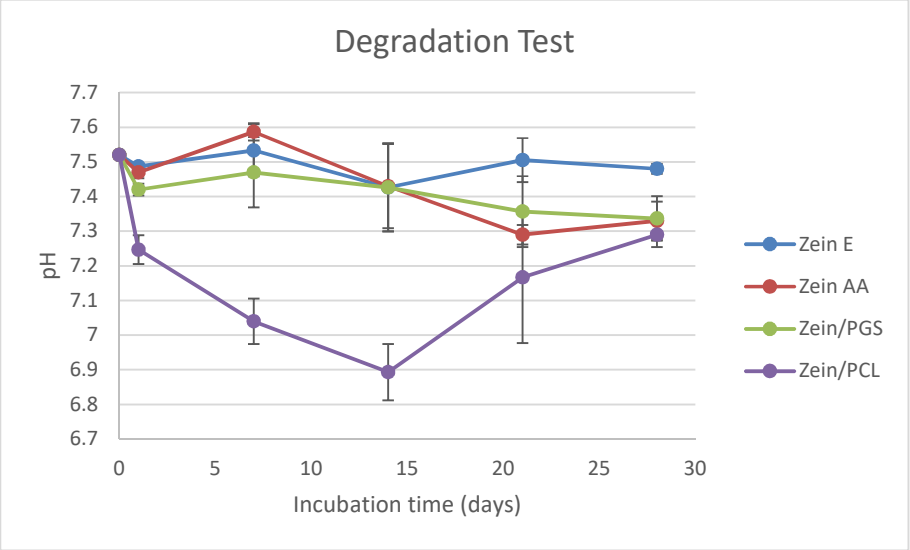

Figure 29. *pH vs. incubation time for the studied samples*

6.3 Microstructural and morphological characterization

6.3.1 Fourier transform infrared spectroscopy (FTIR)

The following figures display FTIR spectra of the samples. Band intensities are expressed as transmittance. This is the ratio of the radiant power transmitted by a sample to the radiant power incident on the sample.

Figure 30 shows the spectra of Zein E before and after the degradation test for each incubation time. The spectrum of three weeks is missing because the samples used for that point degraded completely. In Table 4 it can be observed the list of the main peaks, functional group assignment and type of vibration.

FTIR spectra shows the most prominent vibrational bands of the protein backbone, consisting of amide A from 3600 to 3100 cm^{-1}, amide I from 1700 to 1600 cm^{-1} and amide II between 1600 and 1500 cm^{-1} [(23)]. Amide I band is the most sensitive spectral region to the protein secondary structural components and represents the C=O stretching vibration. In contrast, the amide II band is due to N-H bending and C-N stretching vibrations [(24)]. The FTIR spectra of Zein E shows the presence of NH group at approximately 3300 cm^{-1}, the C-N stretching band at ~1650 cm^{-1} and C=O stretching band at ~1530 cm^{-1}. Those are the characteristic peaks of pure zein reported in the literature [(18)].

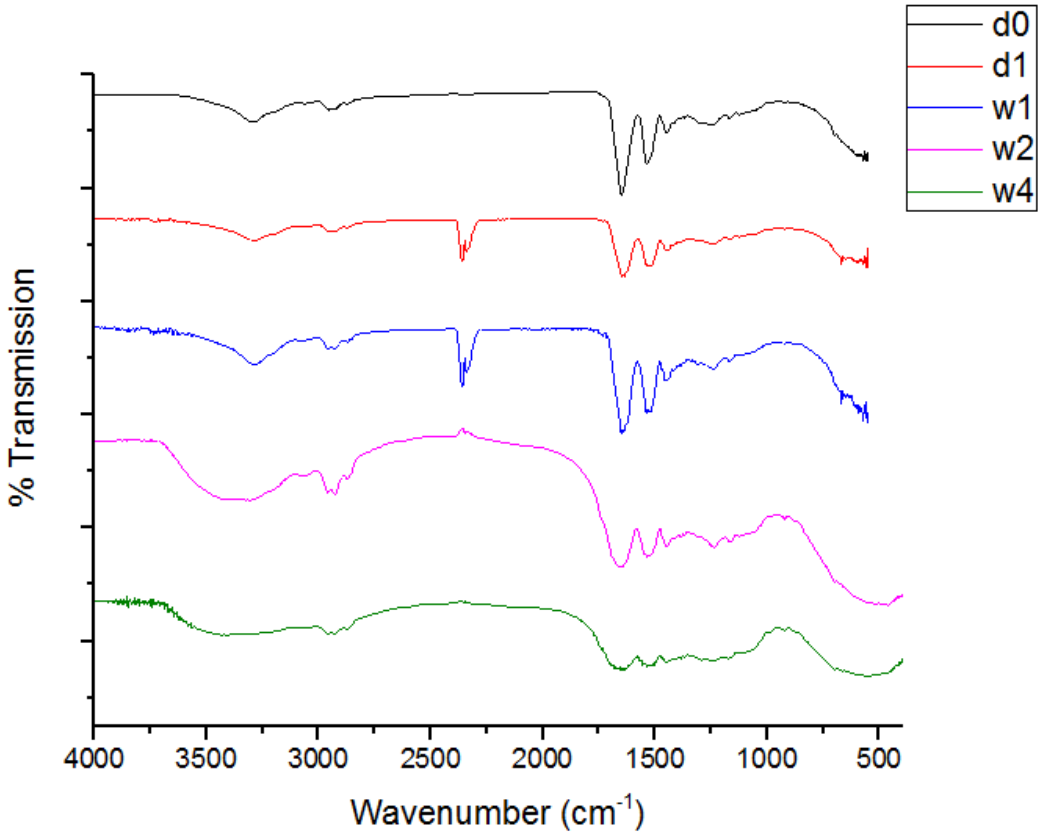

Figure 30. *FTIR spectra for Zein E as a function of degradation time*

Incubation time (days)	Wavenumber (cm^{-1})	Functional group	Type of vibration
0	3299	N-H	Stretch

	1645	C-N	Stretch
	1531	C=O	Stretch
1	3288	N-H	Stretch
	1645	C-N	Stretch
	1531	C=O	Stretch
7	3288	N-H	Stretch
	1649	C-N	Stretch
	1531	C=O	Stretch
14	3373	N-H	Stretch
	1653	C-N	Stretch
	1531	C=O	Stretch
28	3436	N-H	Stretch
	1659	C-N	Stretch
	1531	C=O	Stretch

Table 4. *Characteristic FTIR peaks for Zein E as a function of degradation time*

With increasing incubation time, the peak of NH group shifts from 3299 to 3288 cm $^{-1}$ and then widens at two and four weeks. This broadening could mean that some interaction occurs, usually due to hydrogen bonding interaction but it can also be attributed to the degradation of the zein.

Regarding the other peaks, C-N group appears at 1645 cm^{-1} for 0 and one day of degradation, but increases in wavenumber with increasing incubation time appearing at 1659 cm^{-1} after 28 days of degradation. Moreover, like NH group, at two and four weeks C-N peak widens.

C=O stretching band, which appears at 1531 cm^{-1} does not change in wavenumber with incubation time but for the last degradation times the peak widens.

All of these variations in the wavenumber at which peaks appear and the widenings are evidence of the degradation process of the protein.

Figure 31 displays the FTIR spectra of Zein AA. In this case, there can be identified the same peaks than for Zein E since the only difference is the solvent used, which evaporates during the electrospinning process. Vibrational bands, amide A, I and II, are present. NH group at 3300 cm^{-1}, the C-N stretching band at ~1650 cm^{-1} and C=O stretching band at ~1530 cm^{-1} were observed. Table 5 lists the peaks with the corresponding functional groups and vibration type.

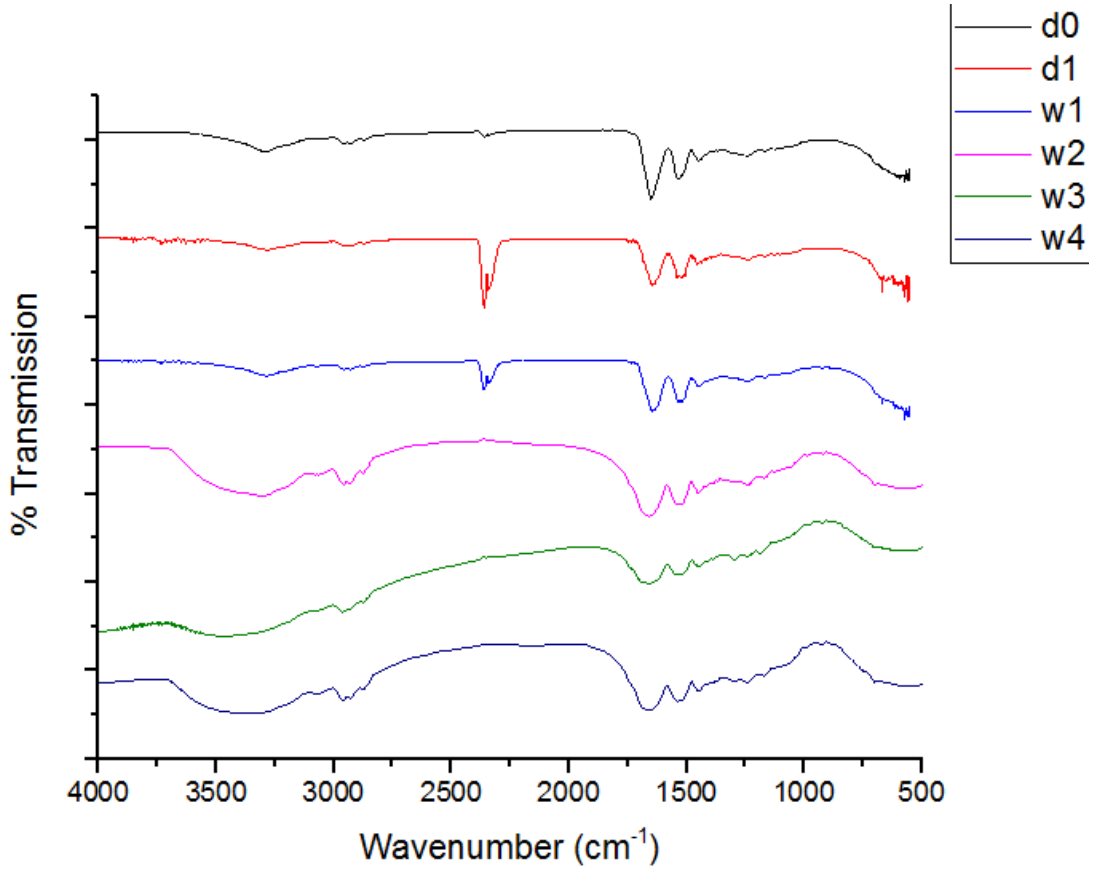

Figure 31. *FTIR spectra for Zein AA as a function of degradation time*

Incubation time (days)	Wavenumber (cm^{-1})	Functional group	Type of vibration
0	3296	N-H	Stretch
	1645	C-N	Stretch
	1537	C=O	Stretch
1	3282	N-H	Stretch
	1645	C-N	Stretch
	1531	C=O	Stretch
7	3282	N-H	Stretch
	1645	C-N	Stretch
	1531	C=O	Stretch
14	3302	N-H	Stretch
	1659	C-N	Stretch
	1531	C=O	Stretch
21	3451	N-H	Stretch

	1659	C-N	Stretch
	1531	C=O	Stretch
28	3432-3297	N-H	Stretch
	1656	C-N	Stretch
	1531	C=O	Stretch

Table 5. *Characteristic FTIR peaks for Zein AA as a function of degradation time*

It can be seen that the peak which presents the greatest variation corresponds to NH group. At the first incubation times, it lays at around 3300 cm^{-1} but as the degradation time increases it shifts to ~3400 cm^{-1} and the widening is even bigger than for Zein E sample.

Regarding C-N peak, it appears at 1645 cm^{-1} until two weeks of degradation, where it shifts to ~1660 cm^{-1}. In this case, there is also a broadening of the peak but not as marked as N-H peak.

As Zein sample, the C=O peak appears at 1531 cm^{-1} and it does not change in the wavenumber at which it appears but it also broadens.

Figure 32 shows the FTIR spectra for the different time points of degradation test of Zein/PGS. In this case, there are combined the characteristic peaks of zein and PGS. It can be distinguished at 3300 cm^{-1} the O-H stretching peak and at ~2950 cm^{-1} the alkane group (C-H), corresponding to PGS. Regarding zein, it appears, at 1650 cm^{-1}, the C-N stretching band and at 1530 cm^{-1} the C=O band.

It was reported that PGS exhibits peaks at 2930 cm^{-1} and 2855 cm^{-1} for alkane C-C groups, at 1740 cm^{-1} an intense band due to C=O stretching and at 1164 cm^{-1} due to C-O stretching, being these last bands for ester linkages confirm that the polymer is a polyester [25]. In this case, the C=O band appears slightly shifted at ~1735 cm^{-1} and the C-O stretching band at ~1170 cm^{-1}.

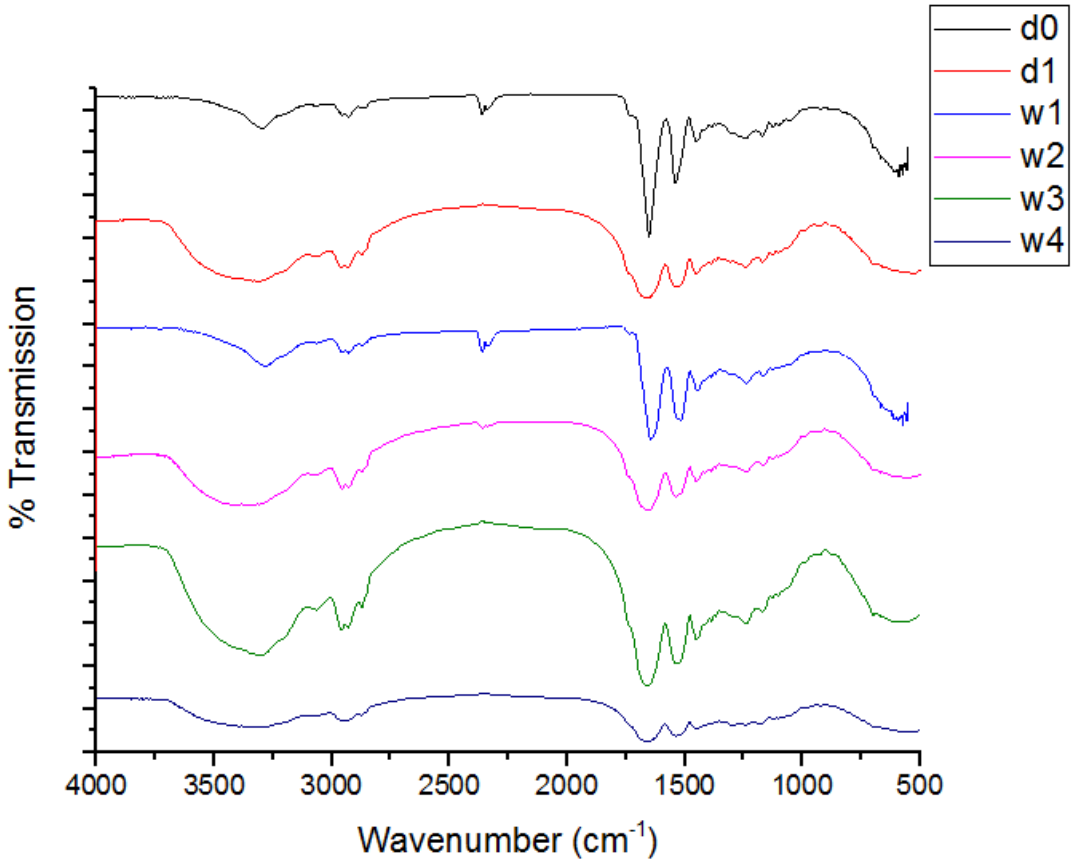

Figure 32. *FTIR spectra for Zein/PGS as a function of degradation time*

Table 6 shows list of peaks with their corresponding functional group and the vibration type for PGS and zein.

Incubation time (days)	**Wavenumber (cm^{-1})**	**Functional group**	**Type of vibration**	
0	3300	O-H	Stretch	PGS
	2957	C-H	Stretch	PGS
	1733	C=O	Stretch	PGS
	1645	C-N	Stretch	Zein
	1537	C=O	Stretch	Zein
	1170	C-O	Stretch	PGS
1	3316	O-H	Stretch	PGS
	2959	C-H	Stretch	PGS
	1735	C=O	Stretch	PGS
	1659	C-N	Stretch	Zein
	1536	C=O	Stretch	Zein

	1170	C-O	Stretch	PGS
7	3288	O-H	Stretch	PGS
	2959	C-H	Stretch	PGS
	2861	C-H	Stretch	PGS
	1735	C=O	Stretch	PGS
	1642	C-N	Stretch	Zein
	1526	C=O	Stretch	Zein
	1170	C-O	Stretch	PGS
14	3367	O-H	Stretch	PGS
	2959	C-H	Stretch	PGS
	1737	C=O	Stretch	PGS
	1659	C-N	Stretch	Zein
	1537	C=O	Stretch	Zein
	1170	C-O	Stretch	PGS
21	3373	O-H	Stretch	PGS
	2961	C-H	Stretch	PGS
	1742	C=O	Stretch	PGS
	1662	C-N	Stretch	Zein
	1534	C=O	Stretch	Zein
	1171	C-O	Stretch	PGS
28	3302	O-H	Stretch	PGS
	2961	C-H	Stretch	PGS
	1738	C=O	Stretch	PGS
	1653	C-N	Stretch	Zein
	1540	C=O	Stretch	Zein
	1183	C-O	Stretch	PGS

Table 6. *Characteristic FTIR peaks for Zein/PGS as a function of degradation time*

The intensity of the characteristic peaks of PGS is not as strong as the observed in zein peaks probably because of the low amount of PGS used for the mats fabrication.

The peak at ~3300 cm^{-1}, which corresponds to O-H stretching, broadens with degradation time. This, as was mentioned before, can be referred to hydrogen bonding interaction as the degradation time increases. Furthermore, it shifts from 3300 to 3373 cm^{-1}.

Regarding literature, at around 2940 cm^{-1} appears the peak related to C-H stretching but in this case, it appears at 2957 cm^{-1} at 0 days of incubation and it shifts to 2961 cm^{-1} after 28 days of degradation.

PGS C=O peak showed the same behavior than the others, with increasing degradation time the peak shifted from 1733 to 1742 cm^{-1} for 21 days of incubation. On the other hand, C=O peak corresponding to zein, remains almost constant at ~1537 cm^{-1}.

Regarding C-O peak, there is a difference with literature where is reported that it appears at 1164 cm^{-1} but in this case, it lays between 1170 and 1180 cm^{-1}. Although in this case intensities are similar, it shifts from ~1170 cm^{-1} (0 and 1 day, 1, 2 and 3 weeks) to 1183 cm^{-1} at four weeks' degradation.

Figure 33 shows FTIR spectra of the blend Zein/PCL. The characteristic band of PCL appears at ~1720 cm^{-1}, corresponding to the C=O stretching of the ester carbonyl group. There can be also identified C-H asymmetric and symmetric stretching at 2940 and 2862 cm^{-1}, respectively. The peaks at ~3300, 1650 and 1540 cm^{-1} correspond to the characteristic absorptions of amide A, amide I and amide II, which are typical protein absorption bands. The last two peaks mentioned are the ones with greater intensity of all.

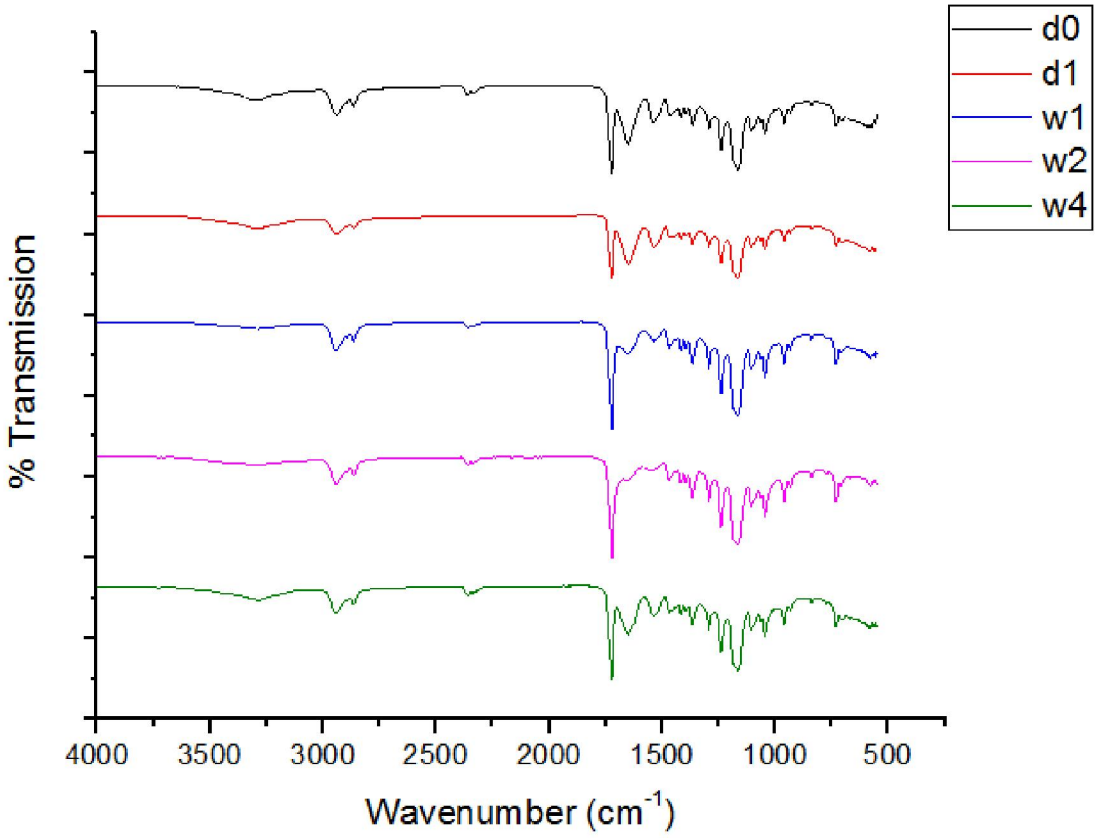

Figure 33. *FTIR spectra for Zein/PCL as a function of degradation time*

In Table 7 there are displayed the characteristic peaks of sample Zein/PCL as a function of degradation time.

Incubation time (days)	Wavenumber (cm^{-1})	Functional group	Type of vibration	
0	3300	N-H	Stretch	Zein
	2940	C-H	Asymmetric stretching	PCL
	2865	C-H	Symmetric stretching	PCL
	1720	C=O	Stretch	PCL
	1650	C-N	Stretch	Zein
	1537	C=O	Stretch	Zein
1	3296	N-H	Stretch	Zein
	2937	C-H	Asymmetric stretching	PCL
	2861	C-H	Symmetric stretching	PCL
	1720	C=O	Stretch	PCL
	1650	C-N	Stretch	Zein
	1535	C=O	Stretch	Zein
7	3284	N-H	Stretch	Zein
	2937	C-H	Asymmetric stretching	PCL
	2861	C-H	Symmetric stretching	PCL
	1721	C=O	Stretch	PCL
	1651	C-N	Stretch	Zein
	1538	C=O	Stretch	Zein
14	3290	N-H	Stretch	Zein
	2940	C-H	Asymmetric stretching	PCL
	2862	C-H	Symmetric stretching	PCL
	1721	C=O	Stretch	PCL
	1658	C-N	Stretch	Zein
	1546	C=O	Stretch	Zein
28	3292	N-H	Stretch	Zein

	2940	C-H	Asymmetric stretching	PCL
	2862	C-H	Symmetric stretching	PCL
	1721	C=O	Stretch	PCL
	1651	C-N	Stretch	Zein
	1542	C=O	Stretch	Zein

Table 7. *Characteristic FTIR peaks for Zein/PCL as a function of degradation time*

It can be noticed that the peaks corresponding to the polymer PCL do not change significantly in wavenumber, evidencing a stronger resistance than zein and PGS. Regarding zein, the peak corresponding to N-H stretching has the greatest variation among zein peaks, as in the cases of Zein E and Zein AA. In respect of C-N peak, it is found at 1650-1651 cm^{-1} with the exception of the sample after two weeks' degradation where it shifts to 1658 cm^{-1} and has the lowest intensity comparing with the other peaks. C=O amide II absorption band shifts from 1537 cm^{-1} to 1542-1546 cm^{-1}. These variations are proof that zein undergoes more degradation than synthetic polymers.

6.4 Mechanical test

It is important to mention that the results do not represent a mechanical property of the materials since the tested samples consisted of randomly oriented fibers. Thus, the obtained values characterize the nanofibrous matrix as a whole and not a single fiber.

The improvement of mechanical properties was investigated by blending of zein with other synthetic polymers and how these properties change with the immersion of the samples in PBS medium.

In Table 7 there are presented the Young's Modulus and tensile strength of Zein AA, Zein/PGS and Zein/PCL before and after the degradation test. For the calculation of the Young's Modulus it was selected the linear region of the stress-strain curve (between approximately 0 and 5% of elongation, whenever possible), eliminating the toe of the curve.

Zein E was not tested due to its brittleness and weakness. Without adding a crosslinking agent, fibers are very brittle, regardless of what concentrations of zein and solvents are used. In alcohol solution, zein protein molecules are not fully stretched or unfolded. The folded polypeptides with large side groups prevents the molecules from getting close enough to each other and to be align and in an

ordered structure. Therefore, it should give a stress-strain curve with typical brittle rupture and fiber breaking tenacity and elongation both low [26].

Before degradation test

Figure 34 shows the stress-strain curve obtained for one of the specimen of Zein AA before the degradation test. Three samples of Zein AA were prepared but two of them were already damaged before testing and the other one broke at the bottom, as can be seen in Figure 35. Therefore, the results correspond to the only sample which finished the test.

It was demonstrated that when zein is dissolved in acetic acid, it is greatly unfolded and intermolecular interpenetration occurs [27]. This means that the mechanical properties of Zein AA should be better than Zein E properties.

It is possible to tailor mechanical properties of zein nanofiber mats by a combination of electrospinning and crosslinking. After zein nanofiber mats are crosslinked, the tensile strength increases significantly and elongation decreases [28]. But Zein AA gave a low Young´s modulus (0.03 MPa) and tensile strength (0.15 MPa) proving that the sample was not crosslinked.

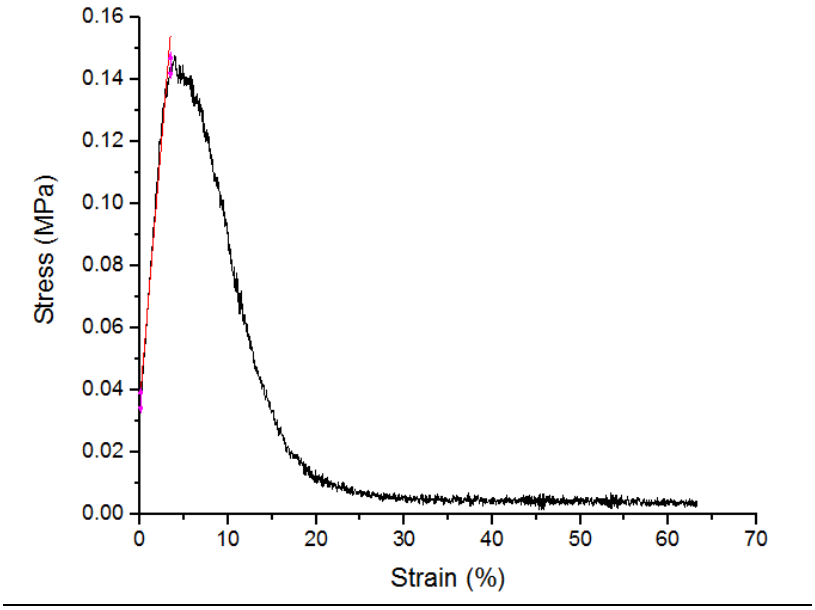

Figure 34. *Stress-strain curve of Zein AA*

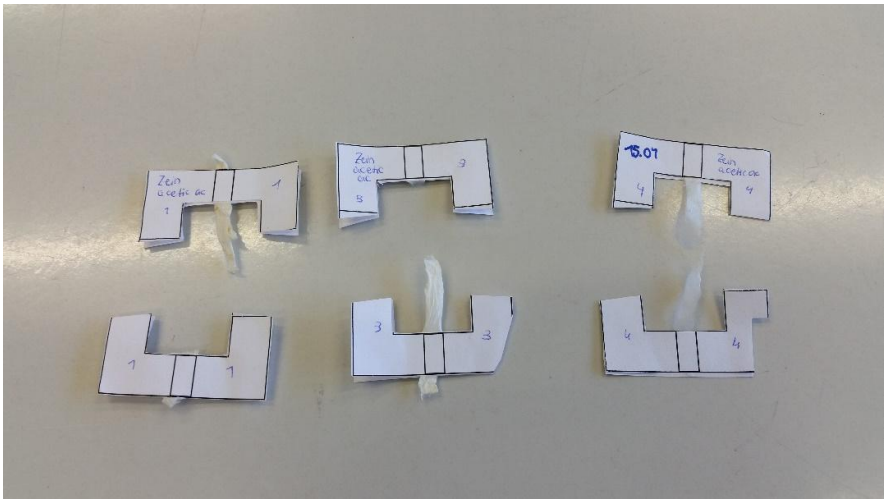

Figure 35. *Zein AA samples after tensile testing*

Figure 36 shows the stress-strain curves of Zein/PGS before degradation test and in Figure 37 it can be seen the samples after the tensile test. In this case, unlike the case before, the samples broke at the middle. Zein/PGS presents a greater ductile character than Zein AA and a higher tensile strength and Young´s modulus. This is evidence that blending zein with a polymer increases mechanical properties. Also, it was proved, in other works, that with the addition of zein, these properties are improved over the value of pure PGS. Zein makes PGS stiffer and mechanically more stable [(18)]. The Young´s modulus obtained was 0.5±0.2 MPa and a tensile strength of 1.4±0.6 MPa. These results are significantly higher than the ones of Zein AA.

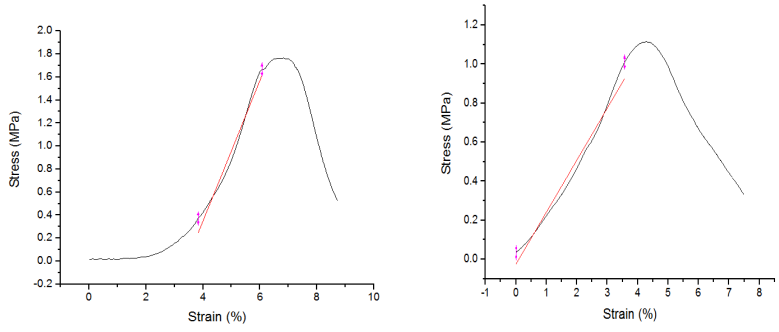

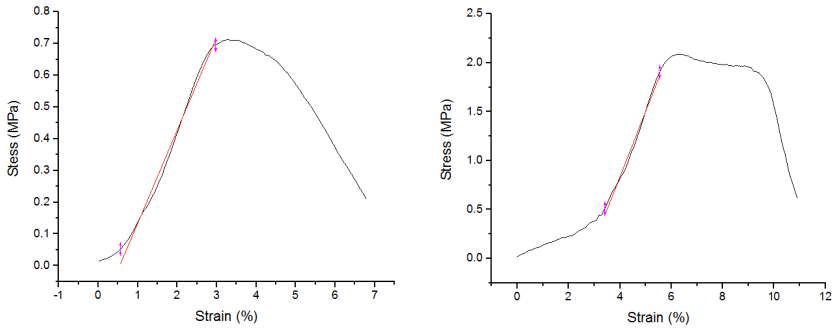

Figure 36. *Stress-strain curves of Zein/PGS*

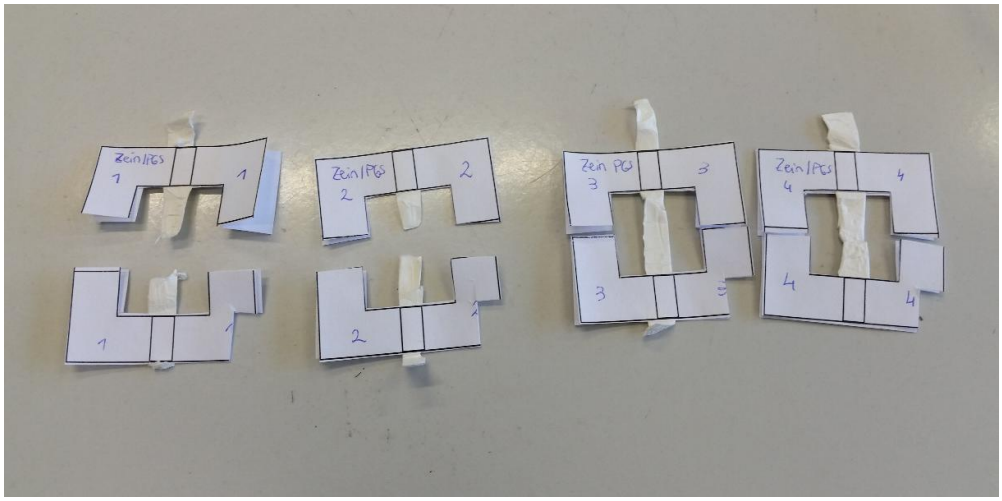

Figure 37. *Zein/PGS samples after tensile testing*

The stress-strain curves of samples Zein/PCL before the degradation test are displayed in Figure 38. In this case, it is shown in Figure 39 that one of the three samples tested broke at the bottom. It was proved that Zein/PCL has more toughness than Zein AA and Zein/PGS and the greatest Young´s modulus and tensile strength, being 0.8±0.5 and 5±3 MPa respectively. Although in other studies it was proven that blends of Zein/PCL reduce resistance compared to pure PCL indicating that they are incompatible [29], in this work it was only compared to Zein AA and Zein/PGS and not with pure PCL.

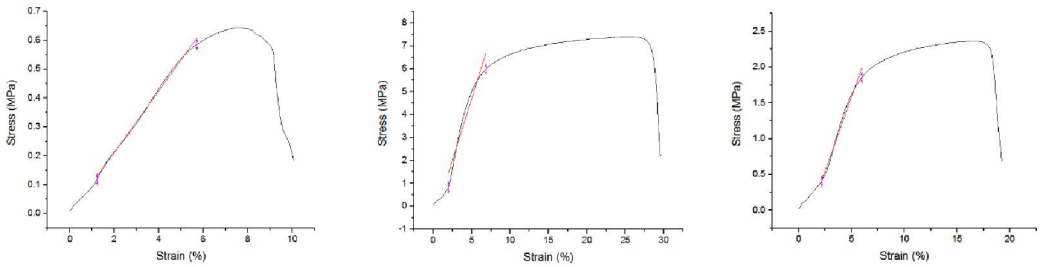

Figure 38. *Stress-strain curve of Zein/PCL*

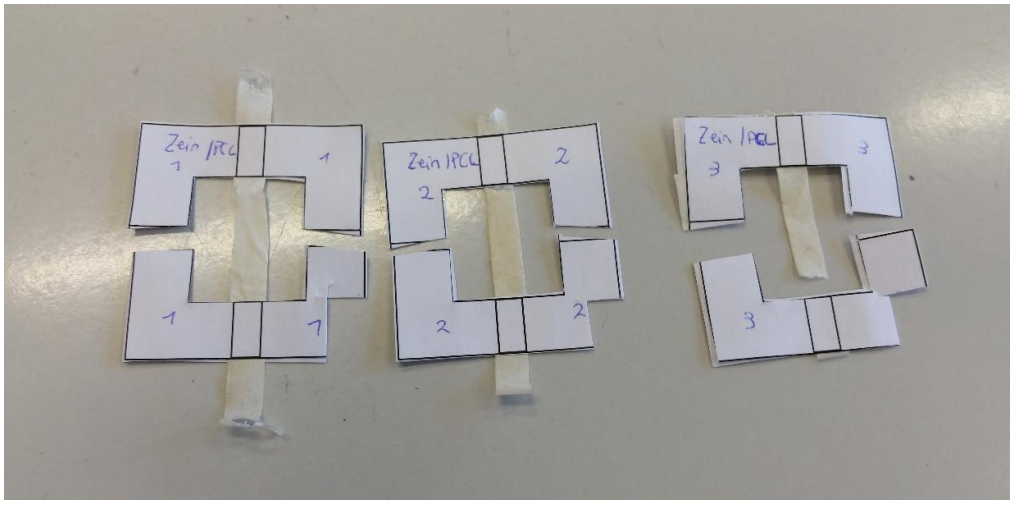

Figure 39. *Zein/PCL samples after tensile testing*

After degradation test

As it was mentioned previously, only sample Zein/PCL was tested after the degradation test. Although Zein/PGS is also blended with a synthetic polymer, after the test the samples were too degraded, making impossible to carry on the mechanical test, as it is shown in Figure 40.

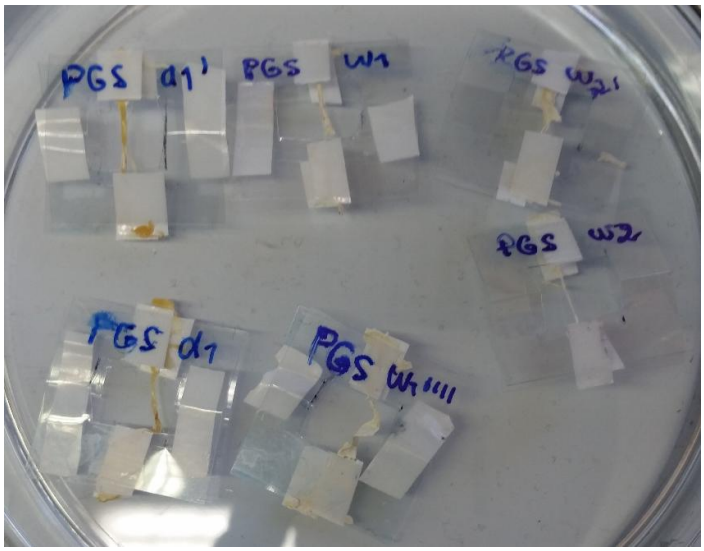

Figure 40. *Zein/PGS samples after degradation test prepared for tensile testing*

Figure 41 shows the three stress-strain curves of Zein/PCL samples after one day of degradation. The ductile behavior is maintained but the Young´s modulus and tensile strength decreased significantly, indicating the evidence of the degradation.

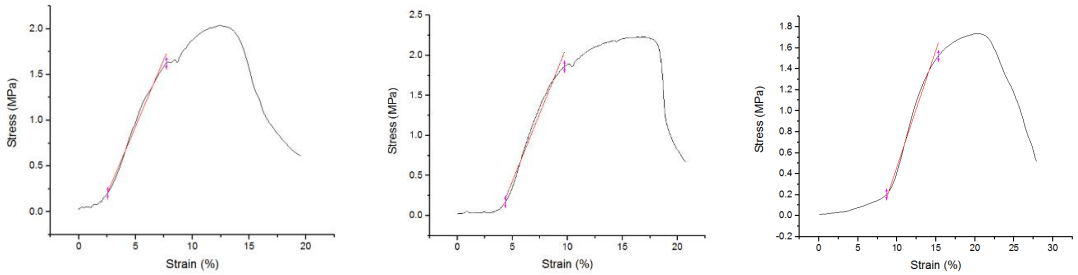

Figure 41. *Stress-strain curve* of Zein/PCL *after one day of degradation*

In Figure 42 it can be seen that among the three samples, only one broke at the middle and the other two at the top.

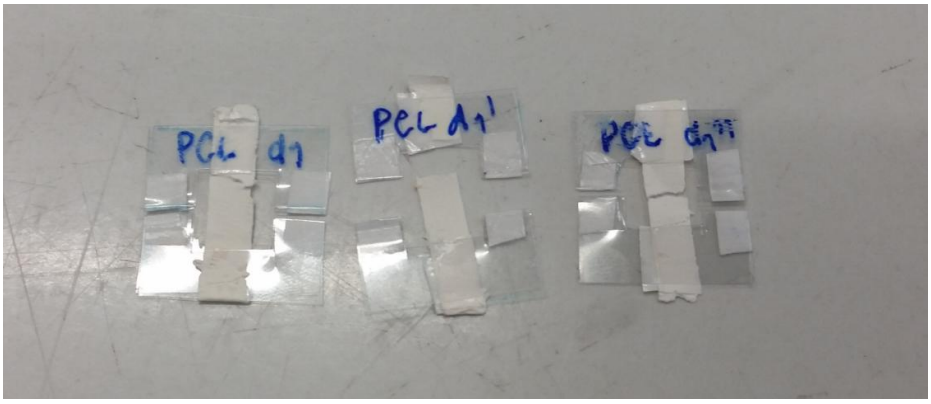

Figure 42. *Zein/PCL samples after tensile test after one day of degradation*

Figure 43 shows the stress-strain curves for Zein/PCL after one week of degradation. The tensile strength in this case was lower than for one day of degradation, which was expected, but the Young's modulus was higher (1.11±0.05 MPa compared to 0.28±0.06 MPa). This difference can be awarded to the fact that the samples were fabricated in different electrospinning runs and probably this sample was more resistant to the degradation test leading to a higher stiffness.

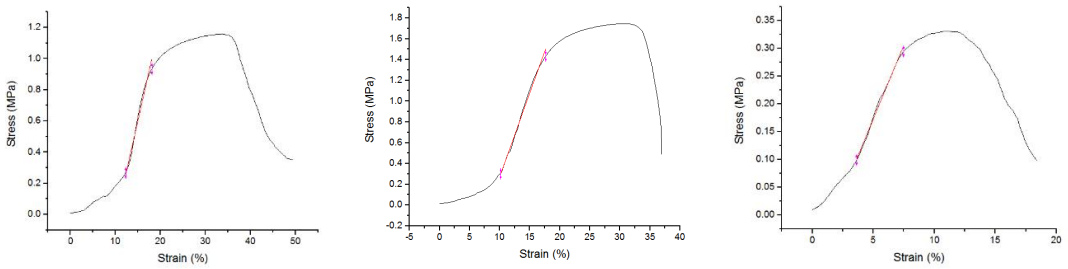

Figure 43. *Stress-strain curve of Zein/PCL after one week of degradation*

In Figure 44 it can be seen that, as in the case before, only one sample broke at the middle.

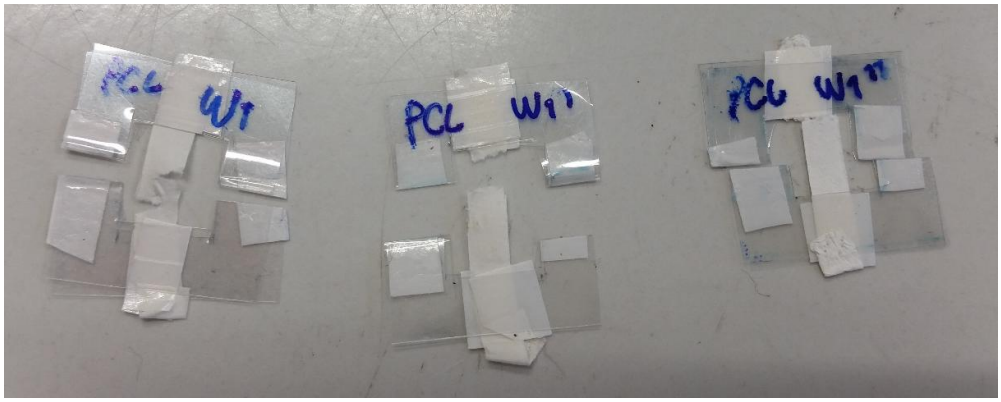

Figure 44. *Zein/PCL samples after tensile test after one week of degradation*

For two weeks of degradation only two samples were tested. Their stress-strain curves are displayed in Figure 45. In this case, as expected, the mechanical properties of the samples were lower than the other incubation time points showing that the properties decrease as the incubation time increases. Figure 46 shows the two samples after the test reveling that only one of them broke at the middle.

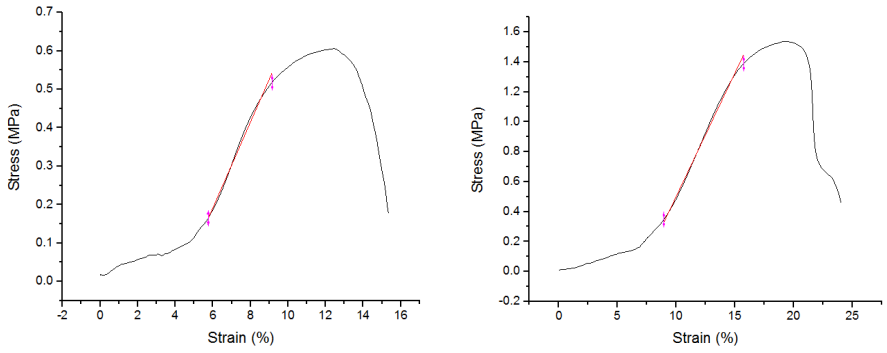

Figure 45. *Stress-strain curve of Zein/PCL after two weeks of degradation*

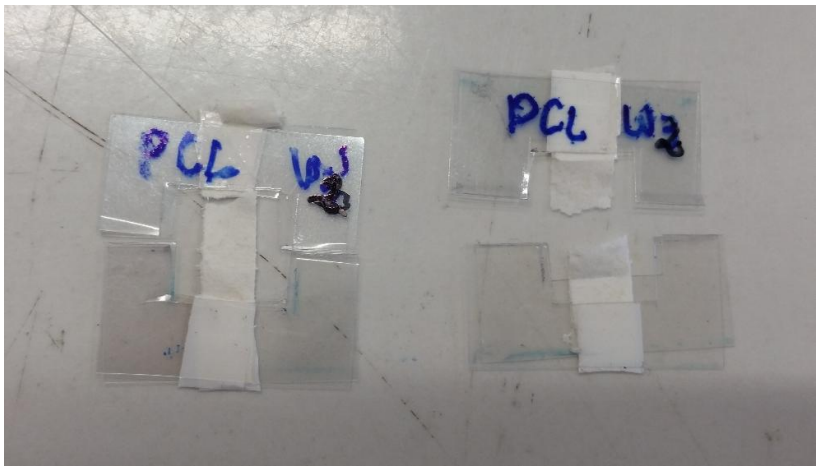

Figure 46. *Zein/PCL with two weeks degradation after tensile test*

Table 8 shows the Young's modulus and tensile strength of the samples before and after degradation test. Summarizing what was mentioned before, the increasing properties order is Zein AA, Zein/PGS and Zein/PCL. Zein/PGS and Zein/PCL had better properties than Zein AA due to the blending with a synthetic polymer, showing Zein/PCL the highest values. It was reported by Jeong et al. that PCL is much stiffer than PGS [30]. Regarding after degradation, the properties showed a decrease in comparison with non-degraded samples.

Sample	**Young´s Modulus (MPa)**	**Tensile Strength (Mpa)**
Before degradation		
Zein AA	0.03	0.15
Zein/PGS	0.5±0.2	1.4±0.6
Zein/PCL	0.8±0.5	5±3
After degradation		
Zein/PCL (1 day)	0.28±0.06	2.0±0.2
Zein/PCL (1 week)	1.11±0.05	1.1±0.7
Zein/PCL (2 weeks)	0.14±0.04	1.1±0.6

Table 8. *Young's Modulus and tensile strength*

7. Conclusions

There were prepared four different nanofibrous scaffolds by electrospinning technique. Although this technique is characterized for its simplicity of process, there are several variables involved which affect the results, such as humidity and temperature which were not controlled in this work.

The crosslinking with citric acid was not successful since fibers were not formed. Solvents such as ethanol and acetic acid were used to investigate the differences with the resulting nanofibrous scaffolds. With the use of acetic acid as solvent, fibers were formed but these scaffolds were not stable during the degradation test. Regarding the other samples, they were electrospun with no other difficulties and processing parameters were adjusted to obtain nanofiber mats.

In electrospinning process it is common to use polymeric solutions in solvent mixtures like chloroform/methanol, methylene chloride/methanol, methylene chloride/N,N-dimethylformamide (DMF), among others [31]. But most of these solvents suitable for electrospinning are toxic and harmful. In this work, the "Green Electrospinning" concept was considered and only benign solvents were used to reduce the disadvantages related to the use of toxic solvents, as environmental impact, safety related issues for the lab work and possible presence of residual toxic solvents in the electrospun mats. With this, the first two objectives raised for this project were successfully accomplished.

Regarding the characterization of the scaffolds, SEM images confirmed the formation of nanofibrous bead-free mats. The fiber diameters had a unimodal distribution, excepting the case of the Zein/PCL sample, where a bimodal distribution size was found and a "net in the net" morphology. Zein/PGS sample presented the lowest fiber diameter whilst Zein/PCL, the greatest. Also, the morphology of the samples was analyzed after degradation showing that Zein/PCL was the most resistant scaffold in the PBS medium. Here, some inconsistencies were found since samples after four weeks of degradation appeared more intact than less incubation times. This was possible because of the way in which the test was conducted (three samples prepared for each incubation time).

The degradation behavior was studied in terms of water uptake, weight loss and pH variations. The results were not as expected and showed a great dispersion. Some samples degraded so the results corresponding to only one specimen are not representative of the behavior. For example, it can be seen in the weight loss graph (Figure 28) that after 28 days of test, the weight loss was less than the previous incubation time, as demonstrated in the SEM images. Increasing the degree of PGS in Zein/PGS sample and crosslinking Zein E and Zein AA, has been suggested as a possible approach to decrease degradation rate [32].

Regarding water uptake, the behavior, in terms of porosity, is in accordance with the morphology that can be seen in SEM images but ideally, the porosity should be measured. Also, it should be analyzed whether the samples have more zein on the surface or polymer, to see if the surface has a

hydrophilic or hydrophobic character. With respect of pH variations, sharp increases or decreases were not found but, in general terms, the degradation of zein generates an increase and degradation products of PCL and PGS, a decrease. Although the changes in pH were small, a minor variation in the surrounding of the present fibrous scaffold could lead to a negative effect on cells [18].

FTIR spectra were used to characterize the samples, confirming the functional groups of each one, and comparing the spectra after degradation it was seen that zein characteristic peaks presented the major changes in wavenumber verifying that synthetic polymers are more resistant to degradation.

Tensile test proved that blending zein with synthetic polymers improves, not only its biocompatibility and degradation resistant, but also, in many folds, its mechanical properties. This test also showed that PCL has more tensile strength than PGS.

With these last characterization test, the final objectives were accomplished although some measurements should be repeated to have more precise results and with minor deviations.

8. References

(1) Nair L. S., Laurencin C. T. “Polymers as biomaterials for tissue engineering and controlled drug delivery”. Advanced biochemical engineering/Biotechnology, 2006, 102, 47-90

(2) Venugopal J., Low S., Choon A. T., Ramakrishna S. “Interaction of cells and nanofiber scaffolds in tissue engineering”. Journal of biomedical materials research, 2008, 84 B (1), 34-48.

(3) Yang S., Leong K. F., Du Z., Chua C. K. “The design of scaffolds for use in tissue engineering. Part I. Traditional factors”. Tissue engineering, 2001, 7 (6), 679-689.

(4) Heisenberg C. P., Bellaiche Y. “Forces in tissue morphogenesis and patterning”. Cell press, 2013, 153(5), 948-962

(5) Frantz C., Stewart K. M., Weaver V. M. “The extracellular matrix at a glance”. Journal of cell science, 2010, 123, 4195-4200.

(6) The Williams dictionary of biomaterials. Liverpool University Press, Liverpool. 1999

(7) O’Brien F.J. “Biomaterials and scaffolds for tissue engineering”. Materials todays, 2011, 14 (3), 88-95.

(8) Wang H.-J., Di L., Ren Q.-S., Wang J.-Y. “Applications and degradation of proteins used as tissue engineering materials”. Materials, 2009, 2, 613-635

(9) Shukla R., Cheryan M. “Zein: the industrial protein from corn”. Industrial crops and products, 2001, 13, 171-192.

(10) Rai R., Tallawi M., Grigore A., Boccaccini A. “Synthesis, properties and biomedical applications of poly(glycerol sebacate) (PGS): A review”. Progress in polymer science, 2012, 37, 1051-1078.

(11) Jiang T., Carbone E. J., Lo K. W.-H., Laurencin C. T. “Electrospinning of polymer nanofibers for tissue regeneration”. Progress in polymer science, 2015, 46, 1-24.

(12) Sill T. J., von Recum H. A. “Electrospinning: Applications in drug delivery and tissue engineering”. Biomaterials, 2008, 28, 1989-2006.

(13) Hohman M. M., Shin M., Rutledge G., Brenner M. P. “Electrospinning and electrically forced jets. I. Stability theory”. Physics of fluids, 2001, 13 (8), 2201-2221.

(14) Garg K., Bowlin G. L. “Electrospinning jets and nanofibrous structures”. Biomicrofluidics, 2011, 5 (1).

(15) Mit-Uppatham C., Nithitanakul M., Supaphol P. “Ultrafine electrospun polyamide-6 fibers: effect of solution conditions on morphology and average fiber diameter”. Macromolecular chemistry and physics, 2004, 205 (17), 2327-2338.

(16) Casper C. L., Stephens J. S., Tassi N. G., Chase D. B., Rabolt J. F. “Controlling surface morphology of electrospun polystyrene fibers: effect of humidity and molecular weight in the electrospinning process”. Macromolecules, 2004, 37 (2), 573-578.

(17) Jiang Q., Reddy N., Yang Y. “Cytocompatible cross-linking of electrospun zein fibers for the development of water-stable tissue engineering scaffolds”. Acta Biomaterialia, 2010, 6, 4042-4051.

(18) Dippold D., Tallawi M., Tansaz S., Roether J. A., Boccaccini A. R. “Novel electrospun poly (glycerol sebacate)-zein fiber mats as candidate materials for cardiac tissue engineering”. European Polymer Journal, 2016, 75, 504-513

(19) Wang H., Di L., Ren Q., Wang J. “Applications and degradation of proteins used as tissue engineering materials “. Materials, 2009, 2, 613-635

(20) Sultana N., Wang M. “Water uptake and diffusion in PHBV tissue engineering scaffolds and non-porous thin films”. Thomson ISI Proceedings, 2011, 11, 24-28.

(21) Müller V., Piai J. F., Ricardo F., Favaro S. L., Rubira A. F., Muniz E.C. “Preparation and characterization of zein and zein-chitosan microspheres with great prospective of application in controlled drug release”. Journal of nanomaterials, 2011.

(22) Paris N., Coffin D.R. “Composition factors affecting the water vapor permeability and properties of hydrophilic zein films”. Journal of agriculture and food chemistry, 1997, 45, 1596-1599.

(23) Forato L.A., De C. Bicudo T, Colnago L.A. “Conformation of α zeins in solid state by Fourier Transform IR”. Biopolymers, 2003, 72, 421-426.

(24) Li Y., Lim L.-T., Kakuda Y. “Electrospun zein fibers as carriers to stabilize (-)-epigallocatechin gallate”. Journal of food science, 2009, 74, 233-240.

(25) Rai R., Tallawi M., Grigore A., Boccaccini A. R. “Synthesis, properties and biomedical applications of poly(glycerol sebacate) (PGS): A review”. Progress in polymer science, 2012, 37, 1051-1078.

(26) Yang Y., Wang L., Li S. “Formaldehyde-free zein fiber preparation and investigation”. Applied Polymer, 1996, 59(3), 433-441.

(27) Yunqi L, Qiuyang X., Shi K., Qingrong H. “Scaling behaviors of α-zein in acetic acid solutions”. The journal of physical chemistry, 2011, 115(32), 9695-9702.

(28) Yao C., Xinsong L., Song T. “Electrospinning and crosslinking of zein nanofiber mats”. Journal of applied polymer science, 2006, 103(1), 380-385.

(29) Corradini E., Mattoso L.H.C., Guedes C.G.F., Rosa D.S. “Mechanical, thermal and morphological properties of poly(ε-caprolactone)/zein blends”. Polymers for advanced technologies, 2004, 15, 340-345.

(30) Jeong C.G., Hollister C.J. “A comparison of the influence of material in vitro cartilage tissue engineering with PCL, PGS and POC 3D scaffold architecture seeded with chondrocytes”. Biomaterials, 2010, 31(15), 4304-4312.

(31) Liverani L, Boccaccini A. R. “Versatile production of poly(epsilon-caprolactone) fibers by electrosspining using benign solvents”. Nanomaterials, 2016, 6 (4), 75.

(32) Wang Y., Ameer G., Langer R. “ Biodegradable polymer”. United States patent application US 2003118692, 2003.

9. Future work

• Repetition of some measurements, especially after degradation, to minimize dispersion and deviation in the results.

• Wettability: Wettability usually involves the measurement of contact angles as the primary data, which indicates the degree of wetting when a solid and liquid interact. The surface of the biomaterial is the first component that comes into contact with the biological cells or fluids. Thus, biocompatibility will be influenced primarily by the surface characteristic of the biomaterial, particularly the wettability, surface chemistry of the exposed atoms, surface energy and the surface topography. Measuring wettability of biomaterials *in vitro* is evaluated by measuring the contact angle at the liquid-solid interface. Furthermore, the knowledge of contact angle gives also information about the hydrophilicity of the material.

• Determination of size and distribution of pores: Porosity structure is one of the most important variables which affect mechanical properties and functionality of the polymeric scaffolds. The regeneration of tissues depends on the grade of porosity, size and shape of pores and continuity or interconnectivity of pores inside the scaffold.

Acknowledgments

I would like to thank my advisors, Dra. Liliana Liverani and Dr. Gustavo Abraham, for sharing their experience and helping me in each step of the work.

I am very grateful to the I.DEAR program which gave me the possibility to spend one year in Germany and allow me to do the final work in a german institute. Specially, thanks to Dra. Silvia Simison, Dr. Aldo Boccaccini and Dr. Flavio Soldera, who oversee the program.

Thanks to the professors and the Universidad Nacional de Mar del Plata, who, during the career, gave me the experience and knowledge needed to face my professional future. Moreover, thanks to Friedrich-Alexander-Universität Erlangen-Nürnberg for letting me make my final work in the Institute of Biomaterials.

Finally, I would like to render thanks to my family and friends who support and helped me during these years.